Dalton Transactions

Accepted Manuscript

ROYAL SOCIETY OF CHEMISTRY

www.rsc.org/dalton

Important Role of Mo-Mo Quintuple Bond in Catalytic Synthesis of Benzene from Alkyne. A Theoretical Study

Yue Chen and Shigeyoshi Sakaki*

ABSTRACT: The Mo-Mo quintuple bond was recently applied to catalytic synthesis of benzene from alkyne, which is the first example of the catalytic reaction of the metal-metal multiple bond. This new reaction was studied using DFT and CASSCF/CASPT2 methods. The entire catalytic cycle consists of four steps: [2+2], [4+2], and [6+2] cycloadditions, and reductive elimination of benzene. The symmetry-forbidden [2+2] cycloaddition and asymmetric [2+2] cycloaddition are two possible pathways for the reaction between alkyne and the Mo-Mo quintuple bond. Though the barrier of the former pathway is moderate because of the presence of the multi-reference character of the Mo-Mo quintuple bond, the asymmetric pathway is much more favorable because of its symmetry-allowed feature. The C-C bond formation in the next [4+2] cycloaddition occurs through the charge transfer (CT) from the π orbital of the incoming alkyne to the π* orbital of another alkyne coordinating with the Mo center to afford a novel dimolybdenacyclic species **3**. In **3**, the $\delta_{d_{xz}}$ and $\delta^*_{d_{xz}}$ orbitals of the Mo-Mo moiety and four π orbitals of the [C_4H_4] moiety construct the π and π* orbitals in the six-member ring. The next [6+2] cycloaddition between **3** and one more alkyne affords an eight-member ring compound **4** which has a Mo-Mo quadruple bond. This is the rate-determining step of the entire catalytic cycle, the $\Delta G^{0‡}$ value of which is 22.4 kcal/mol. The subsequent reductive elimination of benzene easily occurs to yield a μ_2-η^2:η^2-benzene dinuclear Mo complex with a Mo-Mo quintuple bond. On the other hand, further [8+2] cycloaddition between **4** and one more alkyne is much more unfavorable than the reductive elimination of benzene. The similar [4+2] process between alkyne and a Cr-Cr quadruple bond is calculated to be difficult, which is consistent with the experimental result that only the Mo-Mo quintuple bond was successfully applied to this reaction. It is likely that the crowded coordination environment and much more stable $\pi_{d_{yz}}$ orbital in the Cr-Cr quadruple bond are responsible for the difficulty in the reaction.

Introduction

Since the first report of the quadruple bond in a dirhenium complex $[Re_2Cl_8]^{2-}$ by Cotton et al.,[1-4] dinuclear metal complexes with a metal-metal multiple bond have been one of the most interesting and attractive research targets in inorganic chemistry, coordination chemistry, and physical chemistry.[5,6] This compound was theoretically investigated with a multi-reference method and now the well understanding of the Re-Re bonding nature has been presented.[7,8] The similar dichromium and dimolybdenum compounds with a metal-metal quadruple bond were also investigated with the multi-reference method.[9-14] In the last decades, the higher metal-metal multiple bonds such as metal-metal sextuple and quintuple bonds have been reported.[15-64] For instance, a sextuple bond of transient diatomic Cr_2, Mo_2, and W_2 compounds was discussed to be formed with five n*d* orbitals and (n+1)*s* orbital.[15-29] The actinide metals are also able to form a metal-metal multiple bond, to which 5*f* orbitals make a contribution interestingly.[30-35] One good example is U_2.[32] Though these diatomic metal species can be isolated only in an inert matrix at a low temperature in general,[19,20] a stable chromium dinuclear complex ArCrCrAr (Ar = C_6H_3-2,6(C_6H_3-2,6-*i*-Pr_2)$_2$) with a quintuple Cr-Cr bond was reported by Power and his co-workers in 2005.[36] Soon after that, several dinuclear metal complexes with a metal-metal multiple bond have been synthesized by Theopold et al.,[37] Power et al.,[38] Tsai et al.,[39-45] and Kempe et al.[46-48] Also, these compounds have been theoretically investigated well,[8-14,32,36,49-64] in which the metal-metal bonding nature and the geometrical feature have been mainly discussed.

Because the metal-metal multiple bond has d_δ and/or d_π bonding orbitals at a high energy and their anti-bonding counterparts at a lower energy, the metal-metal multiple bond is expected to exhibit high reactivity. However, the reaction of the metal-metal multiple bond has not been reported until recent several pioneering works: Kempe, Theopold, and Tsai groups reported interesting reactions of the dichromium complexes with $AlMe_3$,[47] N_2O, RN_3,[65] NO,[66] P_4, As_4, AsP_3,[67] group 16 and 17 elements,[68] and alkynes.[69-71] Especially, the reaction with alkynes is of considerable interest. The dichromium complexes $Cr_2(^HL^{iPr})_2$ ($^HL^{iPr}$ = N,N'-bis(2,6-*i*$Pr_2C_6H_3$)-1,4-diazadiene)[70] and $Cr_2(\eta^2$-DMePyNDipp)$_2$

(DMePyNDipp = 6-(2, 6-$Me_2C_6H_3$)pyridine-2-yl(2, 6-*i*PrC_6H_3)amide)[69] bearing a Cr-Cr quintuple bond (Scheme 1) react with alkyne through [2+2] cycloaddition to afford a metallacyclic compound with a four-member ring. Also, $Cr_2(\eta^2$-DMePyNDipp$)_2$ reacts with diene to provide a μ-η^1:η^2-coordinated metallacyclic complex through [2+4] cycloaddition. Though all these reactions are stoichiometric, Tsai and coworkers recently reported an interesting catalytic synthesis of benzene derivative by a dinuclear molybdenum complex Mo_2(N^N)$_2$ (N^N = N,N'-$(DipN)_2CH$, Dip = 2,6-*i*$Pr_2C_6H_3$) **1** (Scheme 1) bearing a Mo-Mo quintuple bond,[71] as shown in Scheme 2. The first step is the [2+2] cycloaddition of alkyne with the Mo-Mo quintuple bond to afford a metallacyclic compound **2** which contains a four-member ring structure like the reaction of alkyne with the Cr-Cr quintuple bond.[71] The second step is the reaction of the metallacyclic compound with the second alkyne to afford a six-member dimolybdenacyclic compound **3** through [2+4] cycloaddition. The species **3** reacts with one more alkyne to produce an intermediate **4** with eight-member ring**,** which corresponds to [2+6] cycloaddition. The final step is the reductive elimination of benzene from **4**. This is the first example of the catalysis by the metal-metal multiple bond, suggesting a large potential of the metal-metal multiple bond for application to organic synthesis. Another interesting finding in this catalytic reaction is the [2+2] cycloaddition reaction of the metal-metal multiple bond with alkyne; though this type of [2+2] cycloaddition is understood not to easily occur in general in the case of organic molecule because of the symmetry-forbidden nature by the Woodward-Hoffmann rule, the Cr-Cr and Mo-Mo quintuple bonds easily undergo the [2+2] cycloaddition with alkyne at low temperature (-35 ℃). The species **3** is also a new compound attracting our interests because it is different from currently known metallabenzenes; note that **3** contains two metal elements in its six-member ring unlike usual metallabenzene which contains one metal atom.[72-74] Hence, its aromaticity, stability, and reactivity are of considerable interests. Though many interesting features are found in this catalytic reaction, no detailed analysis has been made yet.

In this work, we theoretically investigated this interesting benzene formation reaction from alkyne catalyzed by **1**. Our purposes here are to (1) explore why the [2+2] cycloaddition reaction between the

Mo-Mo quintuple bond and alkyne easily occurs despite of the symmetry-forbidden character, (2) characterize the electronic structures, bonding natures, and reactivities of metallacyclobutadine **2** and dimolybdenacyclic compound **3**, (3) elucidate how **3** reacts with one more alkyne to complete a full catalytic cycle, and (4) uncover why the Cr analogue of **1** cannot perform this catalytic reaction. Our final goal is to theoretically clarify the origin of the high reactivity of the Mo-Mo quintuple bond.

Model and Computational Details

Geometry optimization was carried out by the DFT method with the B3PW91 functional, in which LANL2DZ basis set with the Los Alamos effective core potentials[75] was used for Mo and 6-31G* basis sets for C, N, and H atoms. This basis set system is named BS-I. The conductor-like polarizable continuum model (CPCM)[76] was applied to the geometry optimization to take solvent effect into account. The harmonic vibrational frequencies were calculated to confirm that the equilibrium structure does not exhibit any imaginary frequency and the transition state has only one imaginary frequency. The potential energy was refined with the B3PW91-D functional with dispersion correction[77] using the above mentioned optimized structure, where large basis set system BS-II was employed; in BS-II, the effective core potentials and basis set by Stuttgart-Dresden-Bonn group[78] were used for Mo and cc-pVDZ for C, N, and H atoms. The Gibbs energy was calculated at 238.15 K (experimental temperature) with the optimized structures, in which translational entropy was corrected with the method developed by Whitesides et al.[79]

Because the multi-reference character must be considered around the transition state of the symmetry-forbidden [2+2] cycloaddition reaction, this reaction process was analyzed by the CASSCF/CASPT2 method. In the active space, fourteen electrons in ten *d* orbitals of two Mo atoms and two π and π* orbitals of acetylene were considered. The electronic structure of **3** was also analyzed by the RASSCF method, in which an active space consisting of 16 electrons and 16 orbitals was employed.

The active space was separated into RAS1 and RAS3, and 4-electron excitations were allowed to occur from RAS1 to RAS3 at most. For CASSCF and RASSCF calculations, BS-II was used.

To reduce computational cost, we employed a reasonable model in which very large substituents (2,6-*i*Pr_2-C_6H_3) on the N^N ligand of **1** were replaced by 2,6-Me_2-C_6H_3. In the CASSCF/CASPT2 and RASSCF calculations, we employed a small model to save CPU time in which the 2,6-*i*-Pr-C_6H_3 substituents were replaced with H atoms. The small model is represented by adding "m" in the superscript.

All DFT calculations were performed with Gaussian 09 program[80] and all CASSCF/CASPT2 and RASSCF calculations were carried out by Molcas 7.6 Program.[81-83]

Results and Discussion

In the catalytic cycle, it is likely that **1** successively reacts with three alkyne molecules, as experimentally proposed; see Scheme 2. The first step is the [2+2] cycloaddition of **1** with alkyne to afford a metallacyclobutadine compound **2**, and the second step is the [4+2] cycloaddition of **2** with the second alkyne to afford a dimolybdenacyclic compound **3**. The third step is the reaction of **3** with the third alkyne to afford an eight-member ring compound **4**. The last step is either the reductive elimination of **4** to afford benzene or further reaction of **4** with one more alkyne leading to the formation of polymer or oligomer. We will successively discuss these steps.

[2+2] cycloaddition between 1 and alkyne: In this section, we will first discuss a symmetric reaction course of [2+2] cycloaddition of **1** with acetylene and then an asymmetric reaction course.

(A) Symmetric reaction course. The optimized Mo-Mo bond length (2.060 Å) of **1** is close to the experimental one (2.019 Å); see Figure S1. Five *d* orbitals ($d_{x^2-y^2}$, d_{xy}, d_{yz}, d_{z^2}, and d_{xz}) of one Mo interact with five *d* orbitals of another Mo to form five bonding molecular orbitals (MOs) ($\sigma_{d_{x^2-y^2}}$, $\pi_{d_{xy}}, \pi_{d_{yz}}, \delta_{d_{z^2}}, \delta_{d_{xz}}$) and five anti-bonding MOs ($\sigma^*_{d_{x^2-y^2}}, \pi^*_{d_{xy}}, \pi^*_{d_{yz}}, \delta^*_{d_{z^2}}, \delta^*_{d_{xz}}$); see Figure S2. The effective bond order (EBO)[30] of the Mo-Mo bond is evaluated to be 4.2 with the

CASSCF-calculated occupation numbers of these MOs. The $\delta_{d_{z^2}}$, $\delta_{d_{xz}}$, $\delta^*_{d_{z^2}}$, and $\delta^*_{d_{xz}}$ MOs of the Mo-Mo moiety are the HOMO-1, HOMO, LUMO, and LUMO+2, respectively, in the single-reference wavefunction. When acetylene approaches the Mo-Mo bond in a symmetric manner where the C-C triple bond is parallel to the Mo-Mo bond, the reaction is symmetry-forbidden by the Woodward-Hoffmann rule; see Scheme 3. We calculated the potential energy surface of this reaction by the broken-symmetry DFT (BS-DFT) method with C_{2V} symmetry, where we employed a small model ($\mathbf{1}^{\boldsymbol{m}}$). As shown in Figure 1A, the energy barrier is moderate (9.7 kcal/mol) against our expectation. At the transition state ($\mathbf{TS1}^{\mathbf{m}}$), the Mo-C distance is about 2.80 Å, which is much longer than the Mo-C bond (2.126 Å) in the C_{2V}-symmetric equilibrium structure $\mathbf{2a}^{\boldsymbol{m}}$; see Figure 1A. In $\mathbf{2a}^{\boldsymbol{m}}$, the Mo-Mo bond order is calculated to be 3.1 with the CASSCF method,[84-87] indicating that the Mo-Mo bond order decreases by about 1.0. This computational result is consistent with our understanding that the Mo-Mo quintuple bond changes to a quadruple bond in this [2+2] coupling reaction in a formal sense. This reaction process is highly exothermic by 30.0 kcal/mol.

To disclose the reason for the low energy barrier, we analyzed the reaction process around the transition state with the CASPT2/SA-CASSCF method. The CASPT2-calculated energy barrier (11.3 kcal/mol) is similar to the BS-DFT calculated value, as shown by Figure 1B; see potential energy surface (red line) of the ground state. The transition state calculated by the CASPT2 is located at the Mo-C distance of 2.76 Å, which is not different very much from the BS-DFT optimized distance. Two configurations, $\varphi_1^2\varphi_3^0$ and $\varphi_1^0\varphi_3^2$, exhibit important contribution to the ground state. The φ_1 contains an Mo-C anti-bonding overlap which consists of the acetylene π_z and the Mo-MO $\delta_{d_{z^2}}$ orbitals, while the φ_3 contains the Mo-C bonding overlap which consists of the Mo-Mo $\delta^*_{d_{z^2}}$ and the acetylene π^*_z orbitals. When acetylene is distant from the Mo-Mo bond, the main configuration is $\varphi_1^2\varphi_3^0$ in the ground state, as expected. As acetylene approaches the Mo-Mo bond, the main configuration changes from the $\varphi_1^2\varphi_3^0$ to the $\varphi_1^0\varphi_3^2$. The first excited state of the A_1 irreducible representation, which is the same representation as the ground state, becomes stable around the transition state, as shown by the blue

line in Figure 1B. In this electronic state, the configuration changes from the $\varphi_1^0\varphi_3^2$ to the $\varphi_1^2\varphi_3^0$ inversely to the change in the ground state. Because the φ_1 is doubly occupied and the φ_3 is empty at the infinite separation between **1** and acetylene, these configuration changes lead to the formation of the Mo-C bond and the cleavage of π bond breaking in the acetylene moiety. As the Mo-C distance decreases from 2.90 Å to the equilibrium one in $\mathbf{2a^m}$, (1) the electron population of the $\delta^*_{d_{z^2}}$ natural orbital increases from 0.378e to 0.802e but that of the $\delta_{d_{z^2}}$ natural orbital decreases from 1.619e to 0.924e (Figure S3), and (2) the electron population of the π_z^* natural orbital increases from 0.081e to 1.127e but the π_z natural orbital decreases from 1.888e to 1.379e, where we employed the linear combination of molecular orbitals (LCMO) analysis of electron distribution;[84-86] see supporting information page S2. These electron population changes arise from the orbital interactions depicted in Scheme 3. With the decrease of Mo-C distance, the Mo-C bonding MO φ_3 becomes more stable and the anti-bonding MO φ_1 becomes more unstable. Thus, the electron population on φ_3 increases but that on φ_1 decreases. As a result, the electron populations on $\delta^*_{d_{z^2}}$ and π_z^* increase but those on $\delta_{d_{z^2}}$ and π_z decrease. These smooth population changes are consistent with the smooth changes of the configuration weights discussed above. It is important to clarify the reason why the configuration smoothly changes here, since it is likely to relate to the moderate activation barrier despite of the symmetry-forbidden character. The energy difference between two configurations ($\varphi_1^2\varphi_3^0$ and $\varphi_1^0\varphi_3^2$) arises from the energy difference between φ_1 and φ_3 MOs. The φ_1 energy becomes higher when the $\delta_{d_{z^2}}$ energy is higher, while the φ_3 energy becomes lower when the $\delta^*_{d_{z^2}}$ energy is lower. In the Mo-Mo quintuple bond, the $\delta_{d_{z^2}}$ exists at a higher energy and the $\delta^*_{d_{z^2}}$ exists at a lower energy because of the weak δ-type interaction between two d_{z^2} orbitals. As a result, the energy difference between the $\varphi_1^2\varphi_3^0$ and $\varphi_1^0\varphi_3^2$ configurations is small, which leads to the smooth configuration changes and the moderate energy barrier.

(B) Asymmetric reaction course. We investigated an asymmetric approaching pathway in which acetylene approaches **1^{m}** without any symmetry. The geometry optimization indicates that acetylene approaches one Mo center of **1^{m}** to afford an acetylene complex **INT1^{m}** without any barrier in both DFT and CASPT2 calculations, as shown in Figure 2A, where the DFT-optimized geometries were employed for the CASPT2 calculations. **INT1^{m}** is understood to be an η^2-coordinate acetylene complex. This reaction course is symmetry-allowed, in which the charge transfer (CT) occurs from the π_z of acetylene to the $\delta^*_{d_{z^2}}$ of the Mo-Mo bond and from the $\delta_{d_{z^2}}$ of the Mo-Mo bond to the π^*_z of acetylene; see Figure 2A. As the Mo-C distance becomes shorter, the electron population of the $\delta_{d_{z^2}}$ smoothly decreases but that of the π^*_z of acetylene smoothly increases, as shown in Figure 2B, apparently indicating that the considerable CT occurs from the $\delta_{d_{z^2}}$ to the π^*_z. This reaction is highly exothermic by 27.8 kcal/mol. In **INT1^{m}**, the two Mo-C distances are 2.107 Å, the Mo-Mo bond becomes longer to 2.164 Å from 2.042 Å, and the N-Mo-N angle significantly decreases to 127º. The CASSCF calculation clearly shows that the Mo-Mo bond order decreases to 3.3 from 4.2, which is similar to that of the symmetry-forbidden reaction.

We evaluated the potential energy surface of this pathway with the large model **1** bearing bulky substitutes (R_1 = 2,6-Me_2-C_6H_3); see Figure S4 for the geometry. As shown in Figure 3, the coordination of propyne with one Mo atom occurs through a transition state **TS1** to afford a Mo-propyne complex **INT1**. Though **TS1** could be optimized with BS-I, it disappears in the DFT/BS-II calculation; E_a = -6.3 kcal/mol and $\Delta G^{0‡}$ = -1.8 kcal/mol at the DFT/BS-II level. The exothermicity is considerably larger (ΔE = -30.2 kcal/mol), which is essentially the same as the computational result with **1^{m}**. In **INT1**, the Mo-Mo bond length increases by 0.092 Å, which is similar to that in the small model described above. Based on these results, it is concluded that the acetylene coordination with the Mo center easily occurs with a negligible small activation barrier.

The η^2-coordinate **INT1** converts to a four-member ring complex **2** through a transition state **TS2**. The $\Delta G^{0‡}$ value is small (3.7 kcal/mol) and the ΔG^0 value is large (-8.6 kcal/mol) relative to **INT1**.

These values are consistent with the experimental observation that the reaction occurs at very low temperature (-35 ℃).[71] In **TS2**, the C-C triple bond rotates round the Mo^1-C^1 axis. As a result, the Mo^1-C^1 distance becomes somewhat longer to 2.172 Å and the Mo^2-C^2 distance becomes considerably shorter to 2.742 Å from 3.374 Å.

In **2**, it is noted that the four-member ring (C^1-Mo^1-Mo^2-C^2) is non-planar with a dihedral angle φ(C^1-Mo^1-Mo^2-C^2) of -25.7º. This φ is close to the experimental value (-28.5º). Because the similar non-planar structure was also reported in the metallacyclic compound of the Cr-Cr multiple bond,[68-71] this non-planar structure is one of the characteristic features of these four-member metallacyclic compounds, which will be discussed below in detail.

Formations of six-member dimolybdenacyclic compound 3. The Mo-Mo quadruple bond of **2** consists of four bonding MOs ($\sigma_{d_{x^2-y^2}}$, $\pi_{d_{xy}}$, $\pi_{d_{yz}}$, and $\delta_{d_{z^2}}$) in a formal sense. The $\pi_{d_{xy}}$ and $\pi_{d_{yz}}$ MOs can interact with the π^* of the second propyne. Because of the presence of bulky substituents of the N^N ligand, the incoming propyne interacts not with the $\pi_{d_{xz}}$ MO but with the $\pi_{d_{yz}}$ MO to afford an intermediate **INT2** through a transition state **TS3a**, as shown in Figure 4. In **TS3a**, the distance between the propyne and the Mo^2 is about 2.43 Å, suggesting that the propyne has not yet completely formed a coordinate bond with the Mo^2. The $\Delta G^{0‡}$ is 4.7 kcal/mol relative to **2**, which is moderately higher than that of the first propyne coordination. This is because the $\pi_{d_{yz}}$ is more stable than the $\delta_{d_{xz}}$ and the steric repulsion with the bulky substituents on the N^N ligand becomes larger in **TS3a** than in **TS2**; note that **TS3a** is more congested than **TS2**. Compared to **2**, the Mo-Mo bond length in **INT2** considerably increases by 0.325 Å and the C-C triple bond of the propyne moiety increases by 0.108 Å, indicating that the CT occurs from the Mo-Mo moiety to the incoming propyne. **INT2** turns into a less stable intermediate **INT3** via a transition state **TS3b**, where one N atom of the N^N ligand dissociates from the Mo^2 center to provide a vacant site and the second propyne moves to this vacant site; see

Figure 4. Starting from **INT3**, the C^3 of the second propyne approaches the C^2 of the first propyne to afford a six-member dimolybdenacyclic compound **3** through a transition state **TS3c**. In **TS3c**, the C^2-C^3 distance deceases to 2.083 Å from 2.852 Å in **INT3** and the N atom of the N^N re-coordinates with the Mo^2 atom. In **3**, the Mo-Mo distance becomes shorter to 2.167Å and the Mo_2C_4 moiety becomes a planar six-member ring, suggesting the presence of aromaticity. Because **3** is a metallacyclic compound with a Mo-Mo quadruple bond, it is neither metallabenzene nor metallabenzyne but a new type of dimetallacyclic compound. We will discuss its electronic structure and bonding nature below in detail. The $\Delta G^{0‡}$ of this C^2-C^3 bond formation is 13.5 kcal/mol and the ΔG^0 is very negative (ΔG^0 = -66.0 kcal/mol) relative to **INT3**.

This elementary step is understood to be the coupling reaction between the C^1-C^2 double bond of **2** and the C^3-C^4 triple bond of the incoming propyne. Hence, the electronic process of this step is interesting. We investigated this step with the IRC followed by CASSCF calculations, where a small model system was employed.[88] When going from the reactant side (IRC = -12.0) to the IRC = -6.0, the C^2-C^3 distance moderately changes; see Figure 5A. Though the NBO charges of the C^1-C^2 and C^3-C^4 moieties change little when going from IRC = -4.0 to IRC = 4.0, the Mo^1 atomic charge somewhat decreases but the Mo^2 atomic charge somewhat increases. These changes in geometry and NBO charge indicate that the important events occur when going form IRC = -4.0 to 4.0. We inspected in the orbital interaction in this reaction stage, as shown in Figure 5B. The C^2-C^3 bonding orbital considerably changes when going from IRC = -2.0 to 2.0, indicating that the π^* MO of the C^1-C^2 moiety interacts with the π MO of the C^3-C^4 moiety. This orbital interaction induces the CT from the C^3-C^4 moiety to the C^1-C^2 moiety, which is consistent with the changes in NBO charge. In **INT3**, the d_{xz} orbital of the Mo^2 becomes more stable in energy than that of the Mo^1, since the N atom dissociates from the Mo^2 center. As a result, a significantly large polarization occurs in the $d_{xz} - d_{xz}$ bonding MO, which increases the Mo^2 d_{xz} orbital population and decreases the Mo^1 d_{xz} population. Along with the C-C bond formation, the dissociated N again approaches the Mo^2 atom to form the Mo^2-N coordinate bond and

thereby the Mo^2 d_{xz} orbital energy becomes similar to the Mo^1 d_{xz}. As a result, the Mo^2 atomic population decreases but the Mo^1 atomic population increases, as shown in Figure 5(B), and finally the two Mo atoms become equivalent.

[6+2] cycloaddition reaction to produce benzene. The next step is the reaction between the third propyne and **3**. Though the Mo-Mo $\pi_{d_{xy}}$ and $\pi_{d_{yz}}$ MOs of **3** can interact with the π^* MO of the incoming propyne through CT interaction, the bulky substituents on the N^N ligand and the congested six-member ring suppress the approach of propyne in both of the yz and xy planes. Because of this congested geometry, one N atom of the N^N ligand must dissociate from the Mo center to form an intermediate **INT4a** through a transition state **TS4a,** as shown in Figure 6. The C-C triple bond length of the incoming propyne somewhat increases by 0.053 Å and the Mo-Mo bond simultaneously increases by 0.038 Å in **INT4a** due to the CT from the Mo-Mo d_{xz}-d_{xz} bonding MO ($\delta_{d_{xz}}$) to the alkyne π^*. The $\Delta G^{0‡}$ of this step is somewhat large (22.4 kcal/mol), which is consistent with the higher reaction temperature in the experiment compared to those of the previous steps. The subsequent C-C bond formation between the incoming propyne and **INT4a** leads to the generation of **INT4b** with a very small $\Delta G^{0‡}$ value of 4.6 kcal/mol. In **INT4b**, an eight-member ring has not been formed yet but a fused ring structure consisting of four-member and six-member rings is found interestingly. Then, the Mo-C bond breaking occurs to induce the ring extension, which leads to the formation of an eight-member ring complex **4** concomitantly with re-coordination of the N atom of the N^N ligand with the Mo center. These two steps both occur facilely; see $\Delta G^{0‡}$ = -4.2 kcal/mol[89] for **TS4c** and 4.6 kcal/mol for **TS4d**, as shown in Figure 6.

Starting from **4**, two reaction pathways are possible; in one, benzene is produced via reductive elimination (blue line in Figure 7) and in another, one more propyne is inserted into the Mo-C bond to produce a ten-member ring which is ring extension (black line in Figure 7). In the reductive elimination, **4** turns into an intermediate **INT5,** in which the 1,3,5-Me_3-C_6H_3 moiety changes its orientation and the

C^1-C^6 distance moderately decreases from 3.612 Å to 3.117 Å. We could not locate the transition state connecting **4** and **INT5**, probably because the potential energy surface is very flat; a linear transit geometry change from **4** to **INT5** shows a flat potential energy surface without a large barrier. Starting from **INT5**, the reductive elimination occurs to afford a product **5** through a transition state **TS5a**. In **TS5a**, the C^1-C^6 distance further decreases to 2.048 Å but it is still considerably longer than that of benzene. In **5**, benzene is completely formed, which interacts with the Mo-Mo moiety through two C-C double bonds. The $\Delta G^{0‡}$ value of this step is 6.9 kcal/mol and the ΔG^0 is -55.3 kcal/mol relative to **4**, indicating that the reductive elimination easily occurs with a moderate activation barrier and a significantly large exothermicity. The optimized geometry of **5** agrees well with the experimental structure.[90] Though the oxidation state of the Mo is decreased by the reductive elimination of benzene, the Mo-Mo distance changes little, against our expectation that the increase in *d* electron number leads to the formation of one $d_\delta - d_\delta$ bonding MO and thereby a shorter Mo-Mo distance. This is because the CT from the Mo-Mo $\delta_{d_{xz}}$ to the benzene π^* weakens the Mo-Mo bond, as discussed previously.[90]

Based on these computational results, it should be concluded that the Mo-Mo multiple bond efficiently catalyzes the benzene formation from three alkyne molecules through facile [2+2], [4+2], and [6+2] cycloadditions followed by the reductive elimination. In all these steps, the Mo-Mo multiple bond plays crucial roles.

Ring extension via [8+2] cycloaddition between 4 and propyne. As mentioned above, we must consider the possibility that **4** reacts with one more propyne to afford a ten-member ring intermediate. If the ring extension reaction further continues, this Mo-Mo complex promotes the oligomerization and/or polymerization of propyne. We investigated here the reaction of one more propyne with **4**. The first step is the coordination of propyne with one Mo center to afford an intermediate **INT6a**, as shown in Figure 7. The $\Delta G^{0‡}$ value is 13.5 kcal/mol and the ΔG^0 is -9.2 kcal/mol, indicating that this reaction can occur thermally but it is more difficult than the reductive elimination of benzene. The following C-C bond

formation occurs with a moderate $\Delta G^{0‡}$ value of 14.4 kcal/mol to generate an intermediate **INT6b** with a ten-member ring structure. This ring extension occurs via the C-C triple bond insertion into the Mo-C bond. Then, **INT6b** isomerizes to another ten-member ring structure **INT6c**. The reductive elimination of 1,3,5,7-tetramethyl-cyclooctatetraene from **INT6c** occurs with a $\Delta G^{0‡}$ value of 13.6 kcal/mol, as shown in Figure 7. Based on these results, it should be concluded that the reductive elimination of benzene occurs more easily than the further reaction of propyne with **4**. Therefore, **1** catalyzes only the synthesis of benzene.

The [4+2] cycloaddition for the Cr-Cr analogue of 2. The reaction between propyne and the Cr-Cr analogue of **2** (**2**^{Cr}) was studied with the DFT method, where the superscript "Cr" means the Cr analogue. In **2**^{Cr}, the dihedral angle φ(C^1-Cr^1-Cr^2-C^2) is -31.4º, which agrees well with the experimental value (-33.6º). The formation of **2**^{Cr} from **1**^{Cr} and propyne is significantly exothermic by -43.9 kcal/mol. The [4+2] cycloaddition between **2**^{Cr} and one more propyne occurs similarly to the Mo system, as follows: Propyne coordinates with **2**^{Cr} to afford a stable intermediate **INT2**^{Cr} via a transition state **TS3a**^{Cr}. The $\Delta G^{0‡}$ value is 14.8 kcal/mol, which is much larger than that (4.7 kcal/mol) of the Mo reaction system; see Figure 8. The $\Delta G^{0‡}$ value of the C-C bond formation is 27.7 kcal/mol, which is also much larger than that (15.5 kcal/mol) of the Mo system. In **TS3a**^{Cr}, the distance between the Cr^2 and the C^3-C^4 bond is about 2.09Å, which is shorter than that of 2.43Å in **TS3a**. The larger coordination barrier of **TS3a**^{Cr} is likely due to (1) the smaller radius of the Cr 3*d* orbital than the Mo 4*d* orbital, which leads to a more congested geometry around the Cr center, and (2) the much more stable $\pi_{d_{yz}}$ (-6.86 eV) in **2**^{Cr} than that (-6.25 eV) in **2**, which is unfavorable for the alkyne coordination with the Cr center.

Based on these results it should be concluded that **1**^{Cr} cannot be applied to catalytic synthesis of benzene from three molecules of alkyne.

Electronic structures and bonding natures of important metallacyclic compounds 2 and 3. In this catalytic cycle, various interesting intermediates are found. Some of them were experimentally observed and their X-ray structures were reported. In particular, **2** and **3** are of considerable interest, because a metallacyclic compound with two transition metal atoms in a ring structure has not been theoretically studied yet to our knowledge. Here, we wish to discuss their interesting geometries and electronic structures.

The characteristic feature of **2** and its Cr analogue $\mathbf{2}^{\mathbf{Cr}}$ is the non-planar four-member C^1-M^1-M^2-C^2 (M = Mo or Cr) ring,[68-71] which is against our expectation that the C^1-C^2 double bond is conjugated with the M-M quadruple bond. To disclose which of steric factor by the bulky R_1 group and the electronic factor is responsible for this non-planar structure, the small model complex $\mathbf{2}^{\boldsymbol{m}}$ with acetylene was analyzed first. Interestingly, both of the non-planar and planar structures could be optimized, where the former is named $\mathbf{2}\boldsymbol{a}^{m}$ and the latter is $\mathbf{2}\boldsymbol{b}^{m}$; see Figure 9. $\mathbf{2}\boldsymbol{a}^{m}$ is considerably more stable than $\mathbf{2}\boldsymbol{b}^{m}$ by 16.9 kcal/mol. These results indicate that the electronic factor is responsible for the non-planar structure of **2**. It is important to elucidate what electronic factor plays a key role in the non-planar distortion.

As shown in Figure 9, another important geometrical feature is found in $\mathbf{2}^{\boldsymbol{m}}$; the N^1-Mo^2-N^2 angle is 98.0º in $\mathbf{2}\boldsymbol{a}^{m}$ but 175.7º in $\mathbf{2}\boldsymbol{b}^{m}$. The electronic structure of $\mathbf{2}\boldsymbol{b}^{m}$ is easily understood in terms of the interaction between **1** and acetylene; see Scheme 4. The π_z of the acetylene interacts with the $\delta_{d_{z^2}}$ to form a bonding φ_{1b} MO and an anti-bonding φ_{2b} MO, and the π_z^* of the acetylene interacts with the $\delta_{d_{z^2}}^*$ to form a bonding φ_{3b} MO and an anti-bonding φ_{4b} MO. The $\delta_{d_{xz}}$ is doubly occupied and the $\delta_{d_{xz}}^*$ is empty in $\mathbf{2}\boldsymbol{b}^{m}$. The orbital interaction between the acetylene and the Mo-Mo multiple bond in $\mathbf{2}\boldsymbol{a}^{m}$ is different from that of $\mathbf{2}\boldsymbol{b}^{m}$, as follows: (1) The π_z^* of the acetylene interacts with the $\delta_{d_{xz}}^*$ to form a bonding φ_{1a} MO and an anti-bonding φ_{2a} MO. (2) The π_z of the acetylene interacts with the $\delta_{d_{xz}}$ to form a bonding φ_{3a} MO and an anti-bonding φ_{4a} MO. And (3) the $\delta_{d_{z^2}}$ is doubly

occupied and the $\delta^*_{d_{z^2}}$ is empty. We note that the main component of the φ_{2a} is the $\delta_{d_{xz}}$ and that of the φ_{4a} is the $\delta^*_{d_{xz}}$. The most important difference is that the bending structure of the $Mo_2(N\hat{}N)_2$ moiety in $\mathbf{2}\boldsymbol{a}^m$ facilitates the CT from the Mo-Mo moiety to the acetylene because the $\delta_{d_{xz}}$ is destabilized in energy by the anti-bonding overlap with the lone pair orbitals of the N^N ligand. Such kind interaction does not exist in $\mathbf{2}\boldsymbol{b}^m$ because of its planar $Mo_2(N\hat{}N)_2$ moiety. As a result, $\mathbf{2}\boldsymbol{a}^m$ is more stable than $\mathbf{2}\boldsymbol{b}^m$.

3 is a new chemical species, which is of considerable interest because of the presence of the Mo-Mo quadruple bond in the ring structure. The MOs of the six-member ring are considerably different between **3** and usual benzene. The $\delta_{d_{xz}}$ and $\delta^*_{d_{xz}}$ MOs of the Mo-Mo moiety and four *p* orbitals of the remaining $[C_4H_4]$ moiety contribute to the π MOs in the six-member ring, as shown in Figure 10. Three of them (π_1, π_2, and π_3) are doubly occupied bonding MO and the remaining three MOs (π^*_4, π^*_5, and π^*_6) are unoccupied anti-bonding MO in a formal sense like benzene. These results suggest the presence of aromaticity in this molecule like benzene. However, several important differences are found in MO between **3** and benzene, as follows: The π_1 does not delocalize on the whole six-member ring but the Mo centers contribute little to this MO, because the Mo *d* orbital exists at a considerably high energy than the $\pi(b_1)$ MO of the $[C_4H_4]$ moiety. The π_2, π_3, π_4^* and π_5^* MOs contain one more node than the corresponding π and π^* MOs of benzene. Another characteristic feature is that the HOMO of benzene is doubly degenerate but that (π_3) of **3** is not. The HOMO consists of the bonding overlap between the $\delta_{d_{xz}}$ orbital of the Mo-Mo moiety and the $\pi(b_1)$ MO of the C_4H_4 moiety; see Figure 10. The d_{xz} component in this MO plays a crucial role to interact with the third acetylene, as was discussed above. In addition to these π and π^* MOs, one d_σ-d_σ bonding ($\sigma_{d_{x^2-y^2}}$) and two d_π-d_π bonding ($\pi_{d_{xy}}$ and $\pi_{d_{yz}}$) MOs are found around the π_3 MO, and their anti-bonding counterparts are found in unoccupied level. Because of the presence of these two d_π-d_π bonding MOs, the six-member

ring of **3** is understood to be similar to a benzyne analogue rather than a benzene; strictly speaking, **3** has one more π orbital than benzyne, which is one of the characteristic features of **3**.

Sekiguchi et al. reported that the Si-Si triple bond of disilylyne RSi≡SiR (R = Si^{i}Pr[CH(SiMe$_3$)$_2$]$_2$) reacts with alkyne to produce disilabenzene; see Scheme 5.[91] The π MOs of disilabenzene are similar to those of benzene but different from those of **3**; see Figure S5. Though **3** resembles disilabenzene in shape, they are different in electronic structure. It is likely that this difference leads to the high reactivity of **3** towards alkyne. Actually, Sekiguchi et al. reported that the reaction between RSi≡SiR and an excess of phenylacetylene at room temperature produces only disilabenzene but the further reaction does not occur, unlike **3**. These results indicate that the d_δ-d_δ and d_π-d_π bonding and anti-bonding MOs in the Mo-Mo moiety are crucial for the high reactivity of **3**. It is likely to conclude that **3** is reactive for further alkyne because it is similar to metallabenzyne rather than metallabenzene.

Conclusions

We investigated the catalytic synthesis of benzene from alkynes by the Mo-Mo quintuple bonded complex **1**, elucidated the reaction mechanism, and analyzed the electronic structures of interesting intermediates by the DFT and CASSCF/CASPT2 methods. Because of the multi-configurational character, the symmetry-forbidden [2+2] cycloaddition between alkyne and the Mo-Mo quintuple bond occurs with a moderate activation barrier. However, another asymmetric reaction occurs with a negligibly small activation barrier in which alkyne interacts with one Mo center in a symmetry-allowed manner. The product **2** of this [2+2] cycloaddition has a non-planar four-member ring structure rather than a planar one. This non-planar structure arises from the electronic effect, especially from the orbital interaction between the π* MOs of alkyne and the d_δ MOs of the Mo-Mo moiety which are destabilized in energy by the anti-bonding overlap with the nitrogen lone pair of the N^N ligand. The [4+2] cycloaddition between **2** and alkyne easily occurs with a small $\Delta G^{0\ddagger}$ value to afford a six-member ring compound **3**. In **3**, the $\delta_{d_{xz}}$ and $\delta^*_{d_{xz}}$ MOs of the Mo-Mo moiety and four π orbitals of the [C$_4$H$_4$]

moiety construct the π and π^* MOs in the six-member ring. Because of these MOs, **3** is aromatic like benzene. In addition, two $d_\pi - d_\pi$ MOs are involved between two Mo atoms, indicating that **3** is close to metallabenzyne rather than metallabenzene. Because of the presence of these $d_\delta - p_\pi$ type π MO, the next [6+2] reaction between **3** and one more alkyne occurs with the moderate $\Delta G^{0\ddagger}$ value of 22.4 kcal/mol to afford an eight-member ring compound **4**. This is the rate-determining step of the whole catalytic cycle. The subsequent reductive elimination of benzene easily occurs and a μ_2-η^2:η^2-C_6H_6 coordinated Mo-Mo complex is formed. The [8+2] cycloaddition between **4** and one more alkyne is much more difficult than the reductive elimination of benzene. In should be emphasized that the $d_\delta - p_\pi$ π MO plays crucial roles in this catalytic cycle.

In the case of the Cr-Cr quintuple bond, the [4+2] cycloaddition needs a much more larger $\Delta G^{0\ddagger}$ value because of the much more stable $\pi_{d_{yz}}$ orbital and the more congested transition state arising from the small radius of Cr atom.

Acknowledgements

This work is financially supported by Grants-in-Aid from the Ministry of Education, Culture, Science, Sport, and Technology through Grants-in-Aid of Specially Promoted Science and Technology (Grant 22000009) and Grand Challenge Project (IMS, Okazaki, Japan). We are also thankful to the computational facility at the Institute of Molecular Science, Okazaki, Japan.

Notes and references

Corresponding Author

sakaki.shigeyoshi.47e@st.kyoto-u.ac.jp

Fukui Institute for Fundamental Chemistry, Kyoto University, Takano-Nishihiraki-cho 34-4, Sakyo-ku,

Kyoto 606-8103, Japan

Electronic Supplementary Information (ESI) available: The electronic structure of Mo-Mo quintuple bond by DFT and CASSCF; Electron population changes along the symmetric approach of acetylene to Mo-Mo quintuple bond by CASSCF (Figure S3); Geometries of the intermediates and transition states optimized by DFT/BS-I (Figure S4); Natural orbitals of disilabenzene (Figure S5). See DOI: 10.1039/b000000x/

1. Cotton, F. A.; Curtis, N. F.; Harris, C. B.; Johnson, B. F. G.; Lippard, S. J.; Mague, J. T.; Robinson, W. R.; Wood, J. S., *Science* 1964, **145**, 1305-1307.
2. Cotton, F. A., *Inorg. Chem.* 1965, **4**, 334-336.
3. Cotton, F. A.; Curtis, N. F.; Johnson, B. F. G.; Robinson, W. R., *Inorg. Chem.* 1965, **4**, 326-330.
4. Cotton, F. A.; Harris, C. B., *Inorg. Chem.* 1965, **4**, 330-333.
5. Cotton, F. A.; Murillo, C. A.; Walton, R. A., *Multiple Bonds between Metal Atoms*. 3rd ed.; Springer Science and Business Media Inc.: New York, 2005.
6. Wagner, F. R.; Noor, A.; Kempe, R., *Nat. Chem.* 2009, **1**, 529-536.
7. Ferrante, F.; Gagliardi, L.; Bursten, B. E.; Sattelberger, A. P., *Inorg. Chem.* 2005, **44**, 8476-8480.
8. Saito, K.; Nakao, Y.; Sato, H.; Sakaki, S., *J. Phys. Chem. A* 2006, **110**, 9710-9717.
9. Kurokawa, Y. I.; Nakao, Y.; Sakaki, S., *J. Phys. Chem. A* 2009, **113**, 3202-3209.
10. La Macchia, G.; Li Manni, G.; Todorova, T. K.; Brynda, M.; Aquilante, F.; Roos, B. O.; Gagliardi, L., *Inorg. Chem.* 2010, **49**, 5216-5222.
11. Brynda, M.; Gagliardi, L.; Roos, B. O., *Chem. Phys. Lett.* 2009, **471**, 1-10.
12. Brynda, M.; Gagliardi, L.; Widmark, P.-O.; Power, P. P.; Roos, B. O., *Angew. Chem. Int. Ed.* 2006, **45**, 3804-3807.
13. Li Manni, G.; Dzubak, A. L.; Mulla, A.; Brogden, D. W.; Berry, J. F.; Gagliardi, L., *Chem. -Eur. J.* 2012, **18**, 1737-1749.
14. Chang, I. Y.; Yu, J.-S. K., *Chem. -Eur. J.* 2012, **18**, 9189-9193.
15. Frenking, G., *Science* 2005, **310**, 796-797.
16. Noor, A.; Kempe, R., *Chem. Rec.* 2010, **10**, 413-416.
17. Morse, M. D., *Chem. Rev.* 1986, **86**, 1049-1109.
18. Weltner, W.; Van Zee, R. J., *Annu. Rev. Phys. Chem.* 1984, **35**, 291-327.
19. Kundig, E. P.; Moskovits, M.; Ozin, G. A., *Nature* 1975, **254**, 503-504.
20. Klotzbuecher, W.; Ozin, G. A., *Inorg. Chem.* 1977, **16**, 984-987.
21. Gupta, S. K.; Atkins, R. M.; Gingerich, K. A., *Inorg. Chem.* 1978, **17**, 3211-3213.

22. Efremov, Y. M.; Samoilova, A. N.; Kozhukhovsky, V. B.; Gurvich, L. V., *J. Mol. Spect.* 1978, **73**, 430-440.

23. Xiao, Z. L.; Hauge, R. H.; Margrave, J. L., *J. Phys. Chem.* 1992, **96**, 636-644.

24. Casey, S. M.; Villalta, P. W.; Bengali, A. A.; Cheng, C. L.; Dick, J. P.; Fenn, P. T.; Leopold, D. G., *J. Am. Chem. Soc.* 1991, **113**, 6688-6689.

25. Casey, S. M.; Leopold, D. G., *J. Phys. Chem.* 1993, **97**, 816-830.

26. Casey, S. M.; Leopold, D. G., *Chem. Phys. Lett.* 1993, **201**, 205-211.

27. Chisholm, M. H.; Macintosh, A. M., *Chem. Rev.* 2005, **105**, 2949-2976.

28. Kant, A.; Strauss, B., *J. Chem. Phys.* 1966, **45**, 3161-3162.

29. Kraus, D.; Lorenz, M.; E. Bondybey, V., *PhysChemComm* 2001, **4**, 44-48.

30. Roos, B. O.; Malmqvist, P.-Å.; Gagliardi, L., *J. Am. Chem. Soc.* 2006, **128**, 17000-17006.

31. Gorokhov, L. N.; Emelyanov, A. M.; Khodeev, Y. S., *High Temp.* 1974, **12**, 1156-1158.

32. Gagliardi, L.; Roos, B. O., *Nature* 2005, **433**, 848-851.

33. Gagliardi, L.; Pyykko, P.; Roos, B. O., *Phys. Chem. Chem. Phys.* 2005, **7**, 2415-2417.

34. La Macchia, G.; Brynda, M.; Gagliardi, L., *Angew. Chem. Int. Ed.* 2006, **45**, 6210-6213.

35. Glukhovtsev, M. N.; Schleyer, P. V., *Isr. J. Chem.* 1993, **33**, 455-466.

36. Nguyen, T.; Sutton, A. D.; Brynda, M.; Fettinger, J. C.; Long, G. J.; Power, P. P., *Science* 2005, **310**, 844-847.

37. Kreisel, K. A.; Yap, G. P. A.; Dmitrenko, O.; Landis, C. R.; Theopold, K. H., *J. Am. Chem. Soc.* 2007, **129**, 14162-14163.

38. Wolf, R.; Ni, C.; Nguyen, T.; Brynda, M.; Long, G. J.; Sutton, A. D.; Fischer, R. C.; Fettinger, J. C.; Hellman, M.; Pu, L.; Power, P. P., *Inorg. Chem.* 2007, **46**, 11277-11290.

39. Tsai, Y.-C.; Hsu, C.-W.; Yu, J.-S. K.; Lee, G.-H.; Wang, Y.; Kuo, T.-S., *Angew. Chem. Int. Ed.* 2008, **47**, 7250-7253.

40. Hsu, C.-W.; Yu, J.-S. K.; Yen, C.-H.; Lee, G.-H.; Wang, Y.; Tsai, Y.-C., *Angew. Chem. Int. Ed.* 2008, **47**, 9933-9936.

41. Tsai, Y.-C.; Lin, Y.-M.; Yu, J.-S. K.; Hwang, J.-K., *J. Am. Chem. Soc.* 2006, **128**, 13980-13981.

42. Tsai, Y.-C.; Chen, H.-Z.; Chang, C.-C.; Yu, J.-S. K.; Lee, G.-H.; Wang, Y.; Kuo, T.-S., *J. Am. Chem. Soc.* 2009, **131**, 12534-12535.

43. Wu, L.-C.; Hsu, C.-W.; Chuang, Y.-C.; Lee, G.-H.; Tsai, Y.-C.; Wang, Y., *J. Phys. Chem. A* 2011, **115**, 12602-12615.

44. Liu, S.-C.; Ke, W.-L.; Yu, J.-S. K.; Kuo, T.-S.; Tsai, Y.-C., *Angew. Chem. Int. Ed.* 2012, **51**, 6394-6397.

45. Huang, Y.-L.; Lu, D.-Y.; Yu, H.-C.; Yu, J.-S. K.; Hsu, C.-W.; Kuo, T.-S.; Lee, G.-H.; Wang, Y.; Tsai, Y.-C., *Angew. Chem. Int. Ed.* 2012, **51**, 7781-7785.

46. Noor, A.; Wagner, F. R.; Kempe, R., *Angew. Chem. Int. Ed.* 2008, **47**, 7246-7249.

47. Noor, A.; Glatz, G.; Müller, R.; Kaupp, M.; Demeshko, S.; Kempe, R., *Nat. Chem.* 2009, **1**, 322-325.

48. Noor, A.; Glatz, G.; Müller, R.; Kaupp, M.; Demeshko, S.; Kempe, R., *Anorg. Allg. Chem.* 2009, **635**, 1149-1152.

49. Chisholm, M. H., *Coord. Chem. Rev.* 2013, **257**, 1576-1583.

50. Dong, H.; Meng, Q.; Chen, B.-Z.; Wu, Y.-B., *J. Organomet. Chem.* 2012, **717**, 108-115.

51. DuPré, D. B., *J. Phys. Chem. A* 2009, **113**, 1559-1563.

52. Fukui, H.; Nakano, M.; Shigeta, Y.; Champagne, B., *J. Phys. Chem. Lett.* 2011, **2**, 2063-2066.

53. Gagliardi, L.; Roos, B. O., *Inorg. Chem.* 2003, **42**, 1599-1603.

54. La Macchia, G.; Aquilante, F.; Veryazov, V.; Roos, B. r. O.; Gagliardi, L., *Inorg. Chem.* 2008, **47**, 11455-11457.

55. La Macchia, G.; Gagliardi, L.; Power, P. P.; Brynda, M., *J. Am. Chem. Soc.* 2008, **130**, 5104-5114.

56. Landis, C. R.; Weinhold, F., *J. Am. Chem. Soc.* 2006, **128**, 7335-7345.

57. Li, Q.; Sa, R.; Wei, Y.; Wu, K., *J. Phys. Chem. A* 2008, **112**, 4965-4972.

58. Llusar, R.; Beltrán, A.; Andrés, J.; Fuster, F.; Silvi, B., *J. Phys. Chem. A* 2001, **105**, 9460-9466.

59. Merino, G.; Donald, K. J.; D'Acchioli, J. S.; Hoffmann, R., *J. Am. Chem. Soc.* 2007, **129**, 15295-15302.

60. Ndambuki, S.; Ziegler, T., *Inorg. Chem.* 2012, **51**, 7794-7800.

61. Roos, B. O.; Borin, A. C.; Gagliardi, L., *Angew. Chem. Int. Ed.* 2007, **46**, 1469-1472.

62. Takagi, N.; Krapp, A.; Frenking, G., *Inorg. Chem.* 2011, **50**, 819-826.

63. Tang, L.; Luo, Q.; Li, Q.-s.; Xie, Y.; King, R. B.; Schaefer, H. F., *J. Chem. Theo. Comput.* 2012, **8**, 862-874.

64. Xu, B.; Li, Q.-S.; Xie, Y.; King, R. B.; Schaefer, H. F., *J. Chem. Theo. Comput.* 2010, **6**, 735-746.

65. Ni, C.; Ellis, B. D.; Long, G. J.; Power, P. P., *Chem.Commun.* 2009, **0**, 2332-2334.

66. Wu, P.-F.; Liu, S.-C.; Shieh, Y.-J.; Kuo, T.-S.; Lee, G.-H.; Wang, Y.; Tsai, Y.-C., *Chem.Commun.* 2013.

67. Schwarzmaier, C.; Noor, A.; Glatz, G.; Zabel, M.; Timoshkin, A. Y.; Cossairt, B. M.; Cummins, C. C.; Kempe, R.; Scheer, M., *Angew. Chem. Int. Ed.* 2011, **50**, 7283-7286.

68. Tamne, E. S.; Noor, A.; Qayyum, S.; Bauer, T.; Kempe, R., *Inorg. Chem.* 2012, **52**, 329-336.

69. Noor, A.; Sobgwi Tamne, E.; Qayyum, S.; Bauer, T.; Kempe, R., *Chem. -Eur. J.* 2011, **17**, 6900-6903.

70. Shen, J.; Yap, G. P. A.; Werner, J.-P.; Theopold, K. H., *Chem.Commun.* 2011, **47**, 12191-12193.

71. Chen, H.-Z.; Liu, S.-C.; Yen, C.-H.; Yu, J.-S. K.; Shieh, Y.-J.; Kuo, T.-S.; Tsai, Y.-C., *Angew. Chem. Int. Ed.* 2012, **51**, 10342-10346.

72. Bleeke, J. R., *Chem. Rev.* 2001, **101**, 1205-1228.

73. Landorf, C. W.; Haley, M. M., *Angew. Chem. Int. Ed.* 2006, **45**, 3914-3936.

74. Fernández, I.; Frenking, G., *Chem. -Eur. J.* 2007, **13**, 5873-5884.

75. Hay, P. J.; Wadt, W. R., *J. Chem. Phys.* 1985, **82**, 299-310.

76. Barone, V.; Cossi, M., *J. Phys. Chem. A* 1998, **102**, 1995-2001.

77. Austin, A.; Petersson, G. A.; Frisch, M. J.; Dobek, F. J.; Scalmani, G.; Throssell, K., *J. Chem. Theo. Comput.* 2012, **8**, 4989-5007.

78. Dolg, M.; Wedig, U.; Stoll, H.; Preuss, H., *J. Chem. Phys.* 1987, **86**, 866-872.

79. Mammen, M.; Shakhnovich, E. I.; Deutch, J. M.; Whitesides, G. M., *J. Org. Chem.* 1998, **63**, 3821-3830.

80. Frisch, M. J.; Trucks, G. W.; Schlegel, H. B.; Scuseria, G. E.; Robb, M. A.; Cheeseman, J. R.; Scalmani, G.; Barone, V.; Mennucci, B.; Petersson, G. A.; Nakatsuji, H.; Caricato, M.; Li, X.; Hratchian, H. P.; Izmaylov, A. F.; Bloino, J.; Zheng, G.; Sonnenberg, J. L.; Hada, M.; Ehara, M.; Toyota, K.; Fukuda, R.; Hasegawa, J.; Ishida, M.; Nakajima, T.; Honda, Y.; Kitao, O.; Nakai, H.; Vreven, T.; Montgomery, J. A., Jr.; Peralta, J. E.; Ogliaro, F.; Bearpark, M.; Heyd, J. J.; Brothers, E.; Kudin, K. N.; Staroverov, V. N.; Kobayashi, R.; Normand, J.; Raghavachari, K.; Rendell, A.; Burant, J. C.; Iyengar, S. S.; Tomasi, J.; Cossi, M.; Rega, N.; Millam, J. M.; Klene, M.; Knox, J. E.; Cross, J. B.; Bakken, V.; Adamo, C.; Jaramillo, J.; Gomperts, R.; Stratmann, R. E.; Yazyev, O.; Austin, A. J.; Cammi, R.; Pomelli, C.; Ochterski, J. W.; Martin, R. L.; Morokuma, K.; Zakrzewski, V. G.; Voth, G. A.; Salvador, P.; Dannenberg, J. J.; Dapprich, S.; Daniels, A. D.; Farkas, O.; Foresman, J. B.; Ortiz, J. V.; Cioslowski, J.; Fox, D. J.

81. Aquilante, F.; De Vico, L.; Ferré, N.; Ghigo, G.; Malmqvist, P.-å.; Neogrády, P.; Pedersen, T. B.; Pitoňák, M.; Reiher, M.; Roos, B. O.; Serrano-Andrés, L.; Urban, M.; Veryazov, V.; Lindh, R., *J. Comput. Chem.* 2010, **31**, 224-247.

82. Veryazov, V.; Widmark, P.-O.; Serrano-Andrés, L.; Lindh, R.; Roos, B. O., *Int. J. Quantum Chem.* 2004, **100**, 626-635.

83. Karlström, G.; Lindh, R.; Malmqvist, P.-Å.; Roos, B. O.; Ryde, U.; Veryazov, V.; Widmark, P.-O.; Cossi, M.; Schimmelpfennig, B.; Neograd y, P.; Seijo, L., *Comput. Mater. Sci.* 2003, **28**, 222-239.

84. Baba, H.; Suzuki, S.; Takemura, T., *J. Chem. Phys.* 1969, **50**, 2078-2086.

85. Fujimoto, H.; Kato, S.; Yamabe, S.; Fukui, K., *J. Chem. Phys.* 1974, **60**, 572-578.

86. Dapprich, S.; Frenking, G., *J. Phys. Chem.* 1995, **99**, 9352-9362.

87. The electron populations of the bonding and anti-bonding MOs of the Mo-Mo bond was analyzed by fragment's MOs method; see ref 84-86.

88. The active space consists of the bonding ($\sigma_{C\text{-}C}$) and its anti-bonding ($\sigma^*_{C\text{-}C}$) orbitals of C^2-C^3 and eight *d* orbitals of Mo atoms.

89. The $\Delta G^{0\ddagger}$ for **TS4c** is 1.7 kcal/mol at DFT/BS-I level.

90. Carrasco, M.; Curado, N.; Maya, C.; Peloso, R.; Rodríguez, A.; Ruiz, E.; Alvarez, S.; Carmona, E., *Angew. Chem. Int. Ed.* 2013, **52**, 3227-3231.

91. Kinjo, R.; Ichinohe, M.; Sekiguchi, A.; Takagi, N.; Sumimoto, M.; Nagase, S., *J. Am. Chem. Soc.* 2007, **129**, 7766-7767.

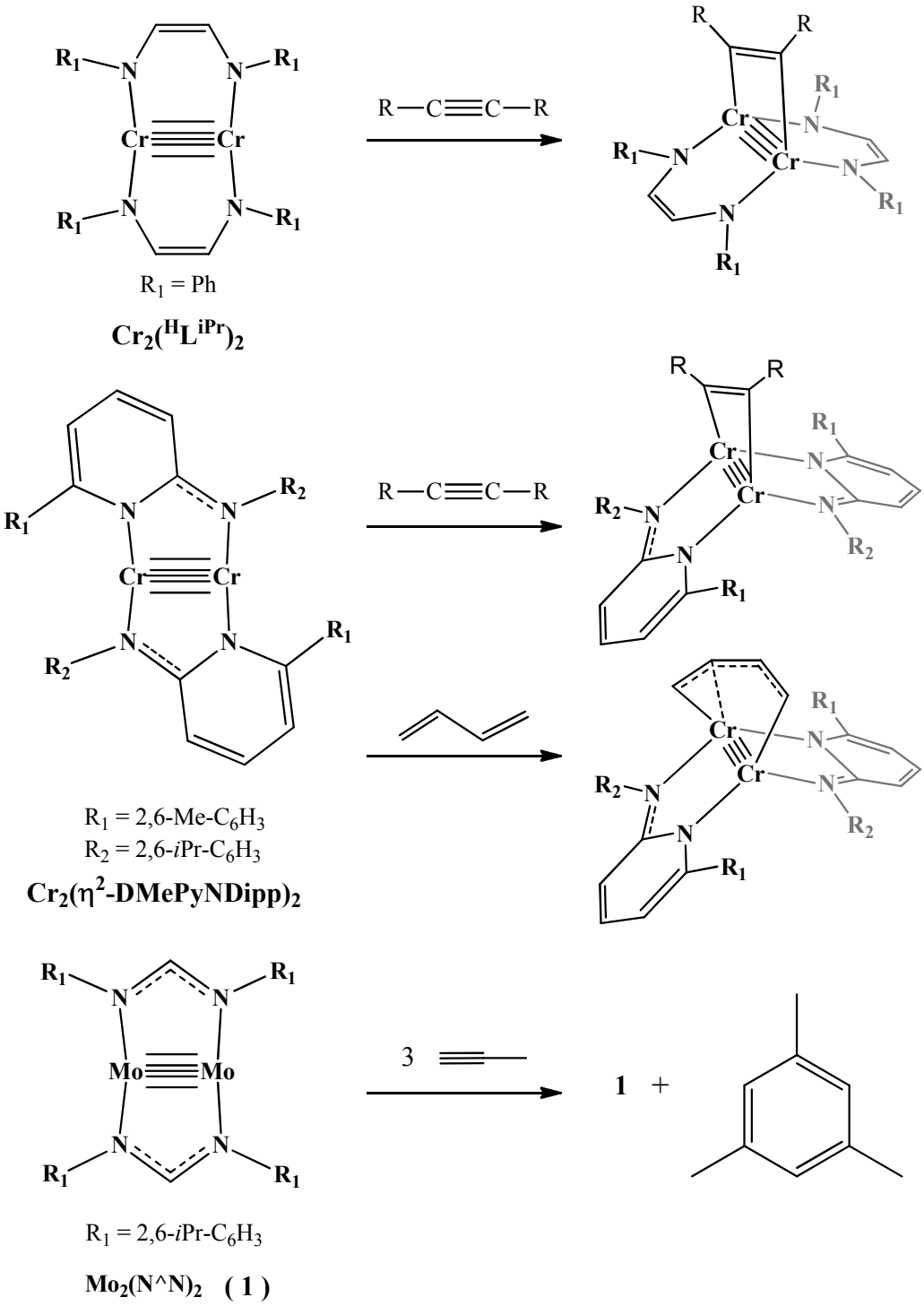

Scheme 1. Various reaction of metal-metal quintuple bond with alkyne.

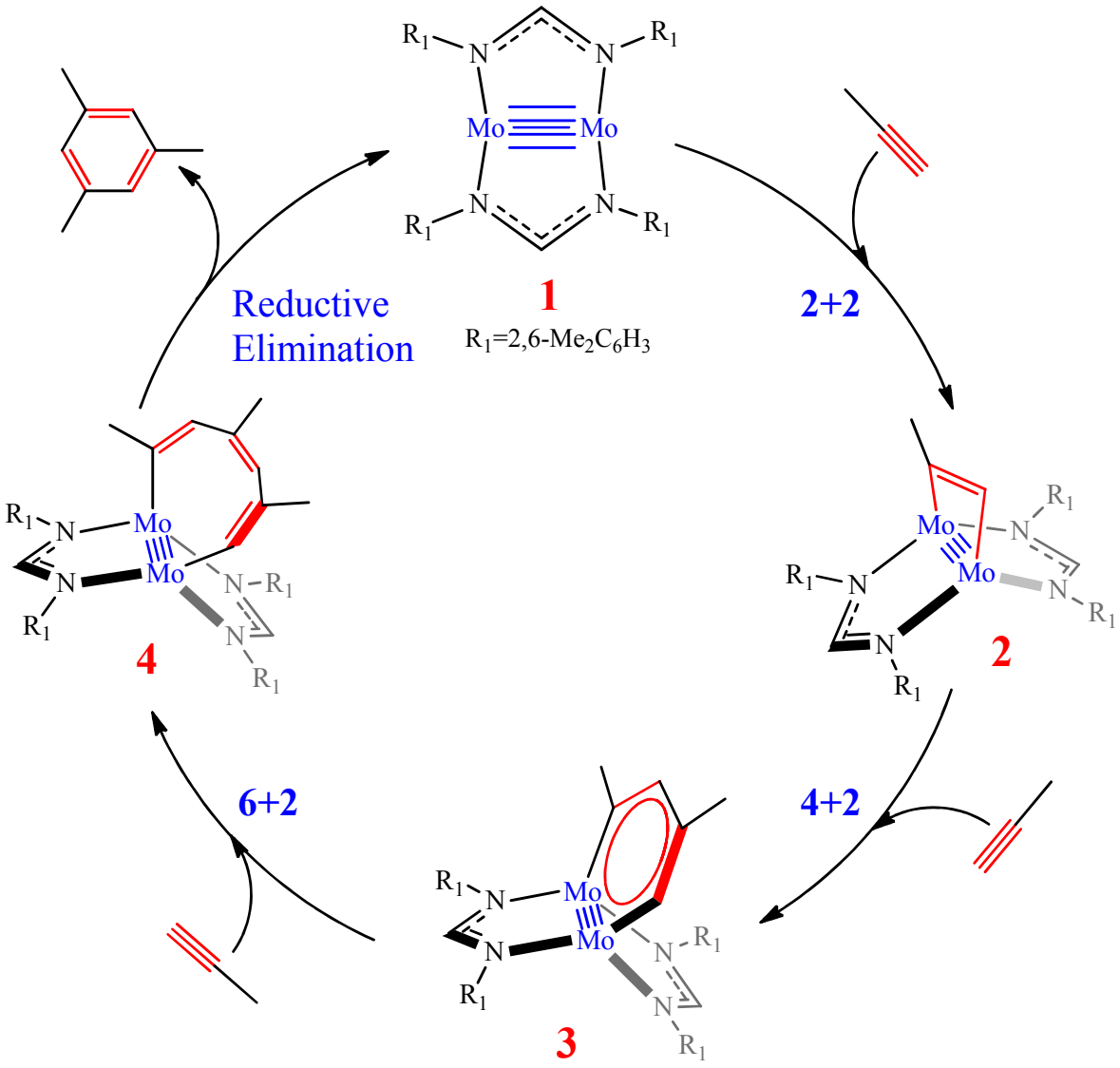

Scheme 2. Proposed catalytic cycle of benzene synthesis from three alkyne molecules by a Mo-Mo quintuple bond.

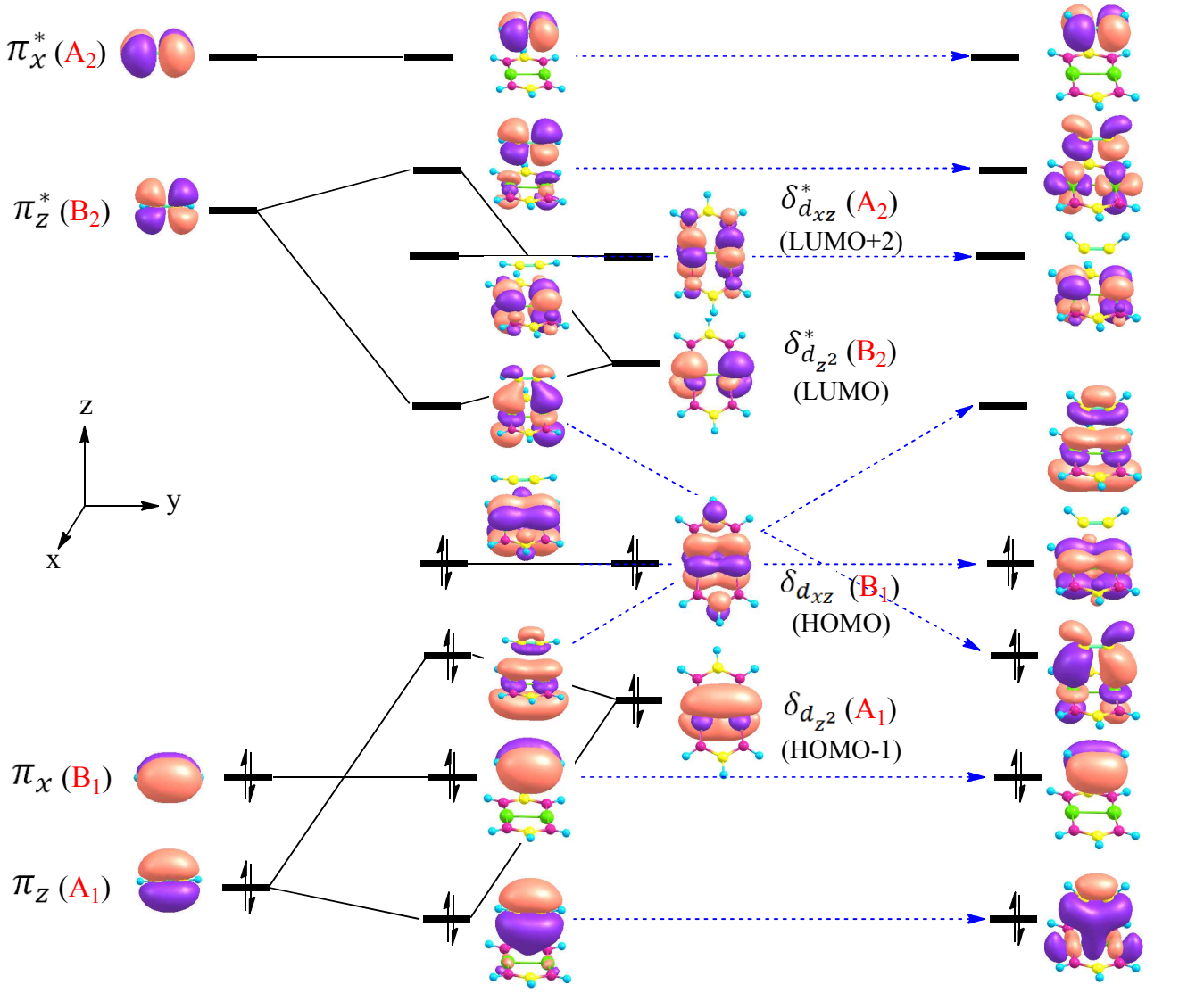

Woodward-Hoffmann Forbidden reaction

Scheme 3. Symmetric approach of acetylene to the Mo-Mo quintuple bond.

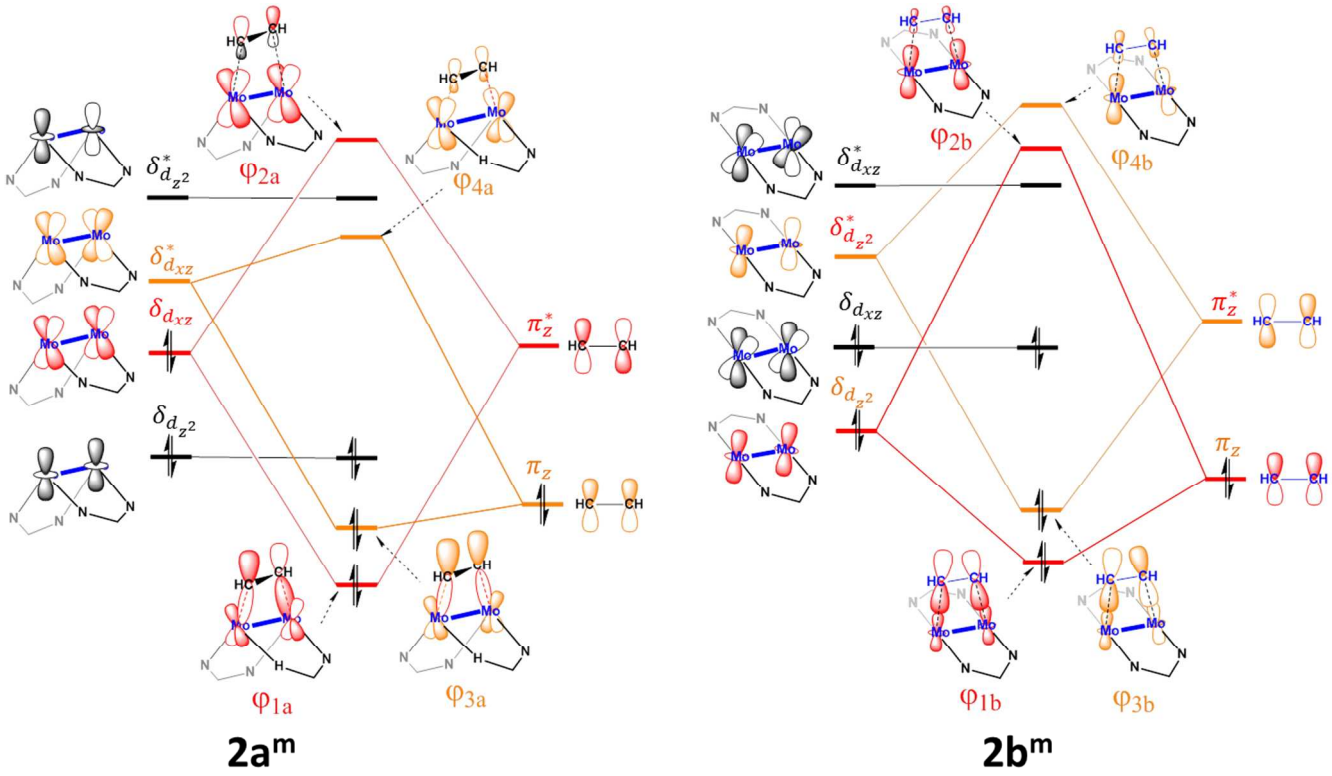

Scheme 4. Orbital interaction in four-member ring compounds **2a**$^{\mathbf{m}}$ and **2b**$^{\mathbf{m}}$.

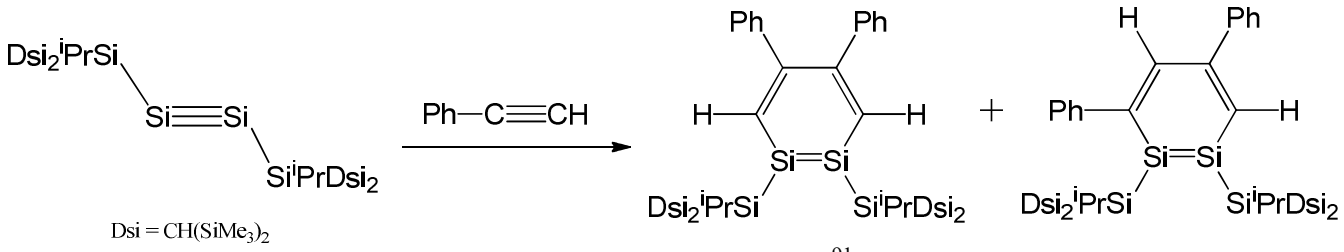

Scheme 5. The reaction between disilylyne and phenylacetylene.[91]

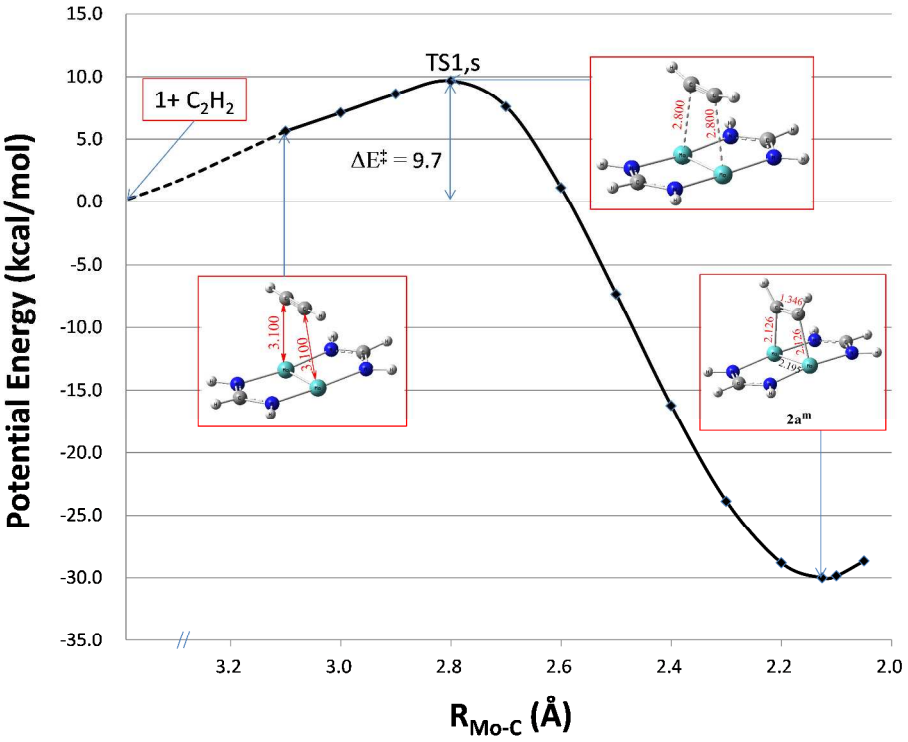

(A)

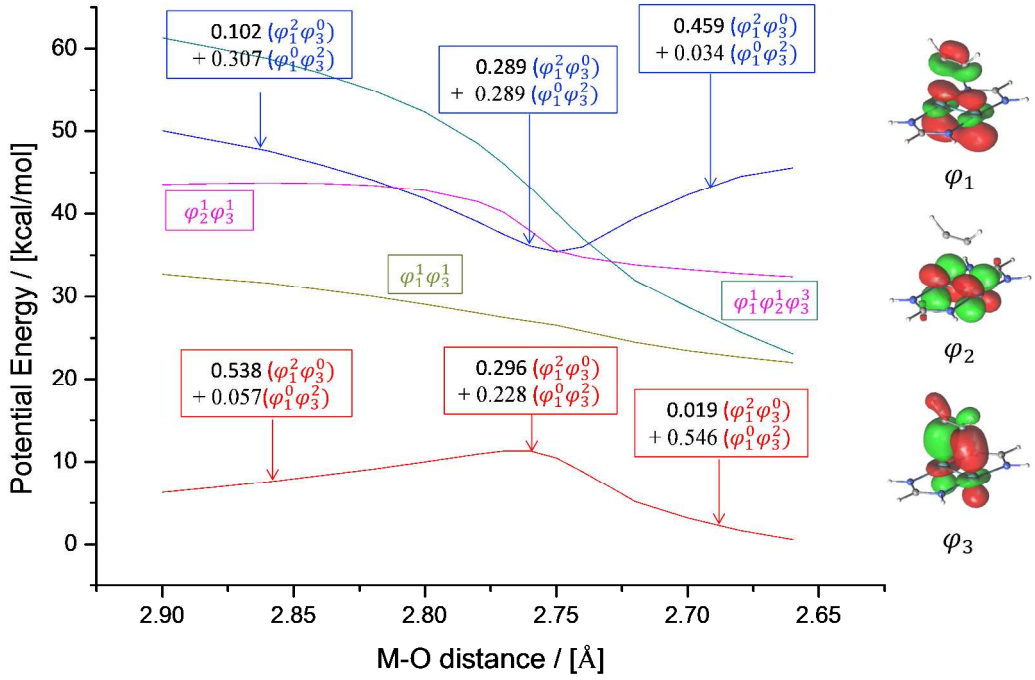

(B)

Figure 1. Potential energy surface of symmetric [2+2] cycloaddition by (A) BS-B3PW91/BS-II, (B) CASPT2/BS-II.

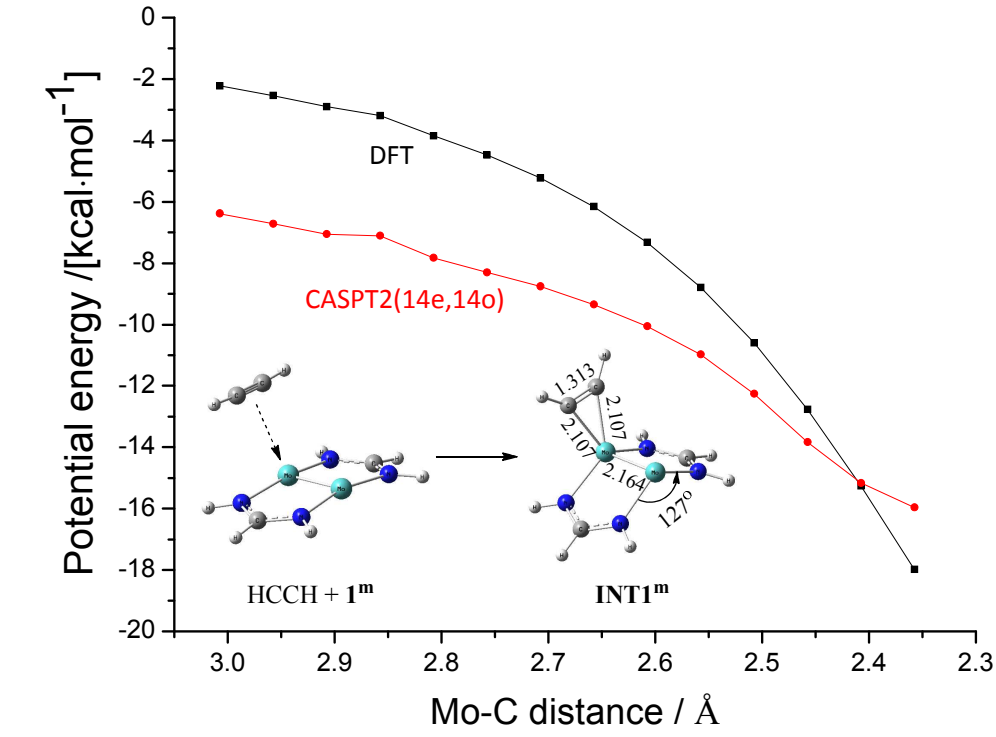

(A)

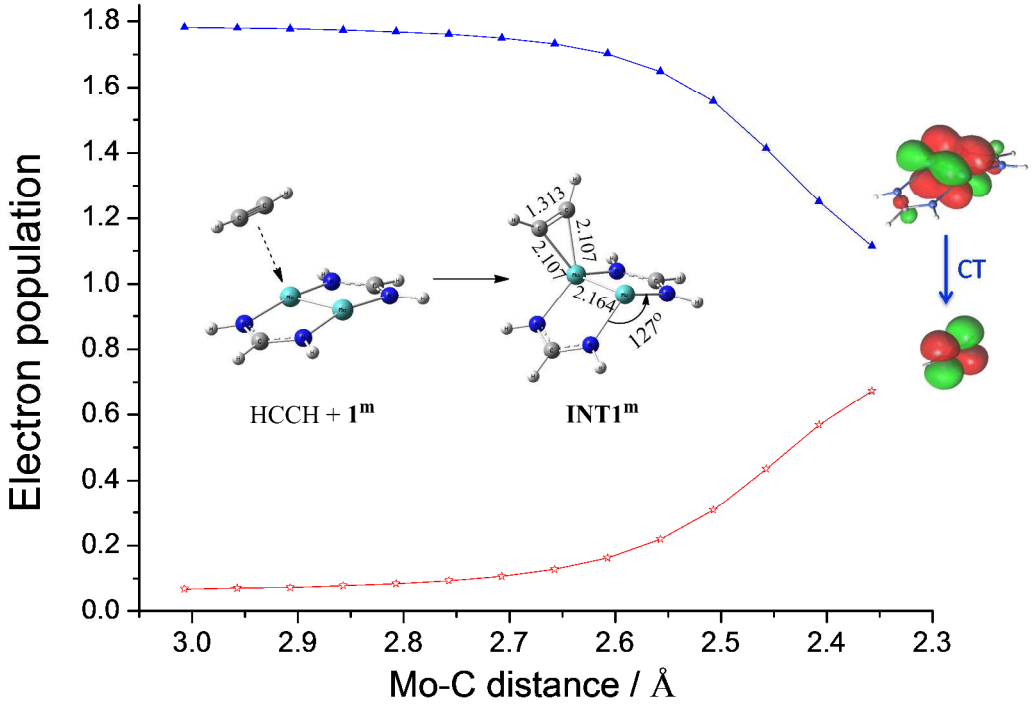

(B)

Figure 2. Potential energy surface of asymmetric approach of acetylene to the Mo-Mo quintuple bond (A) and electron population changes of relevant orbitals (B).

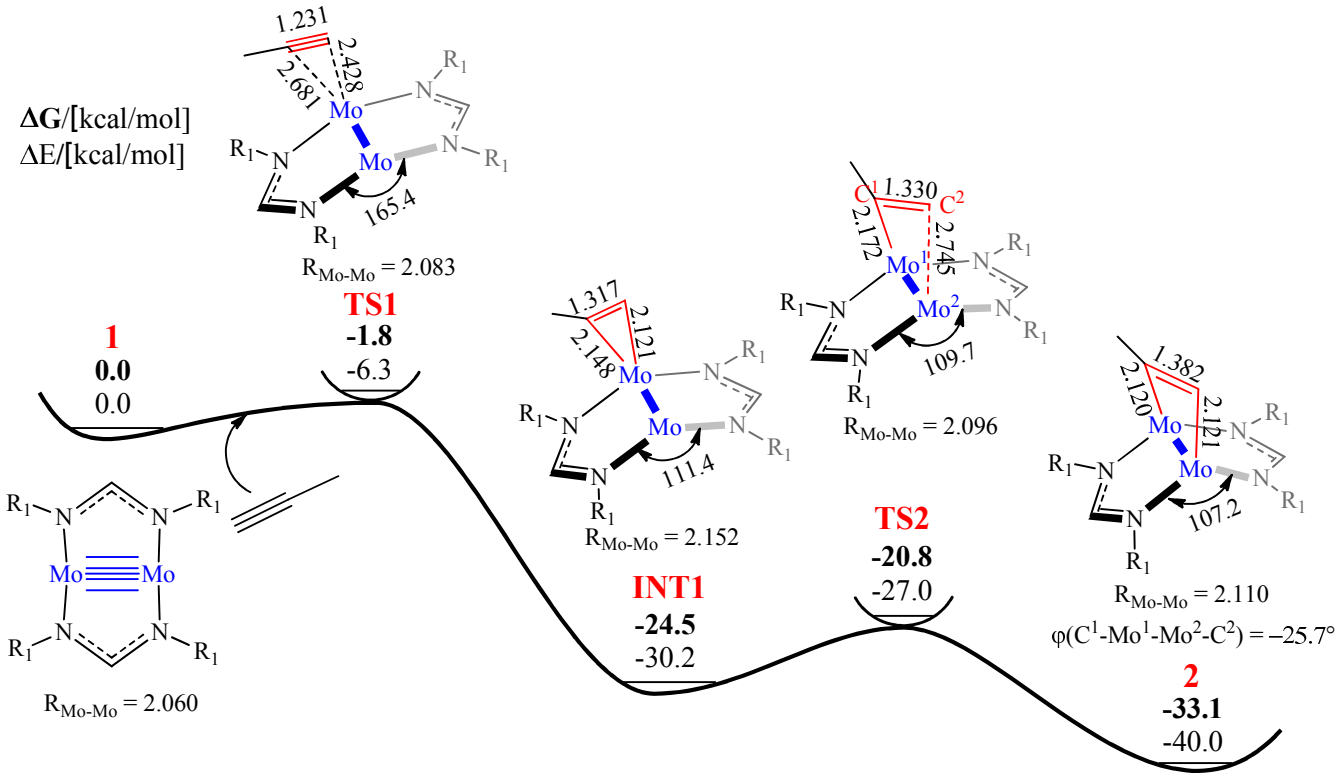

Figure 3. Energy change in the [2+2] cycloaddition via an asymmetric pathway

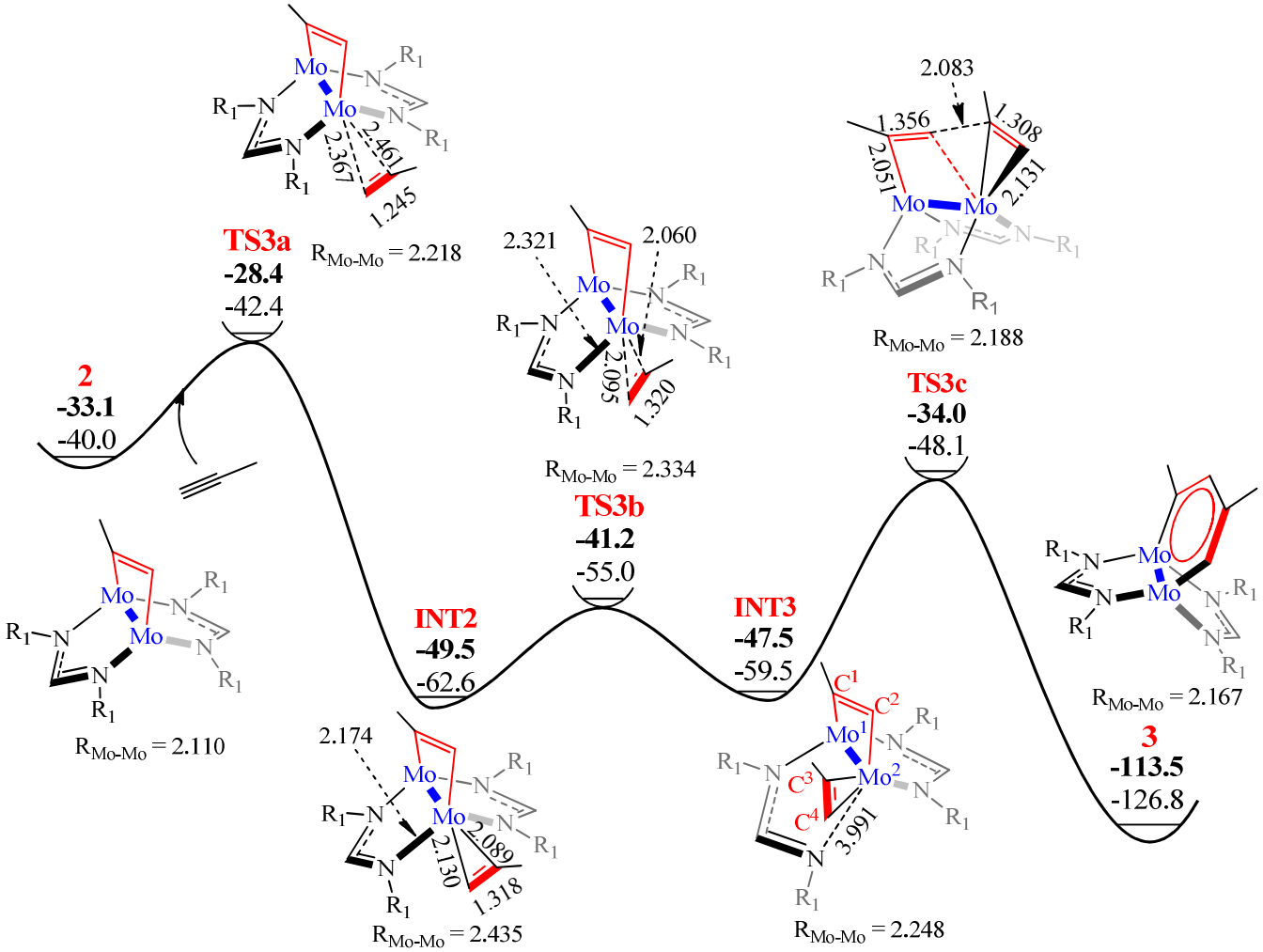

Figure 4. Energy change in the [4+2] cycloaddition between **2** and propyne.

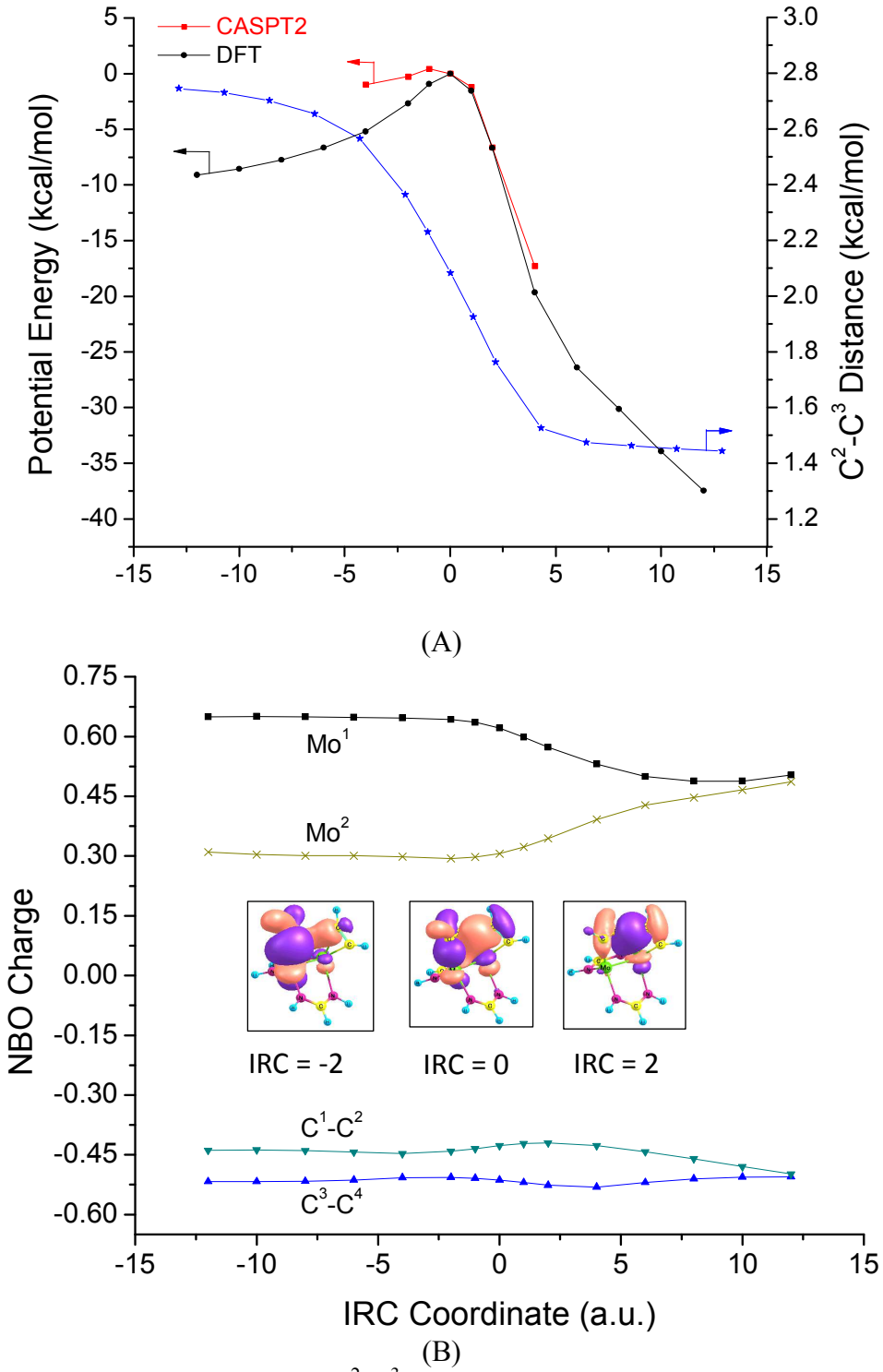

Figure 5. The changes of potential energy, C^2-C^3 distance (A), and NBO charge (B) along IRC of the C-C bond formation.

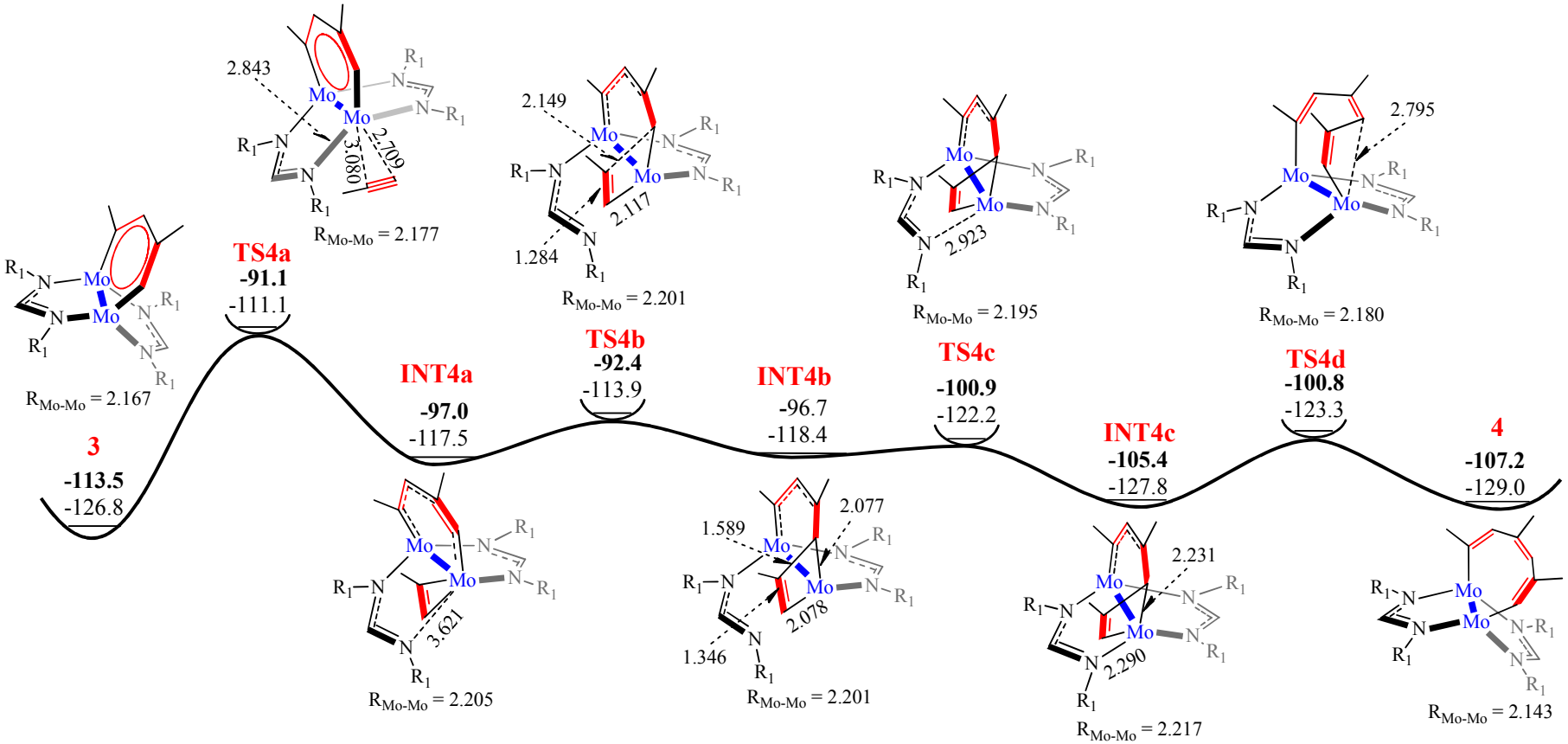

Figure 6. The energy change in the [6+2] cycloaddition between **3** and propyne.

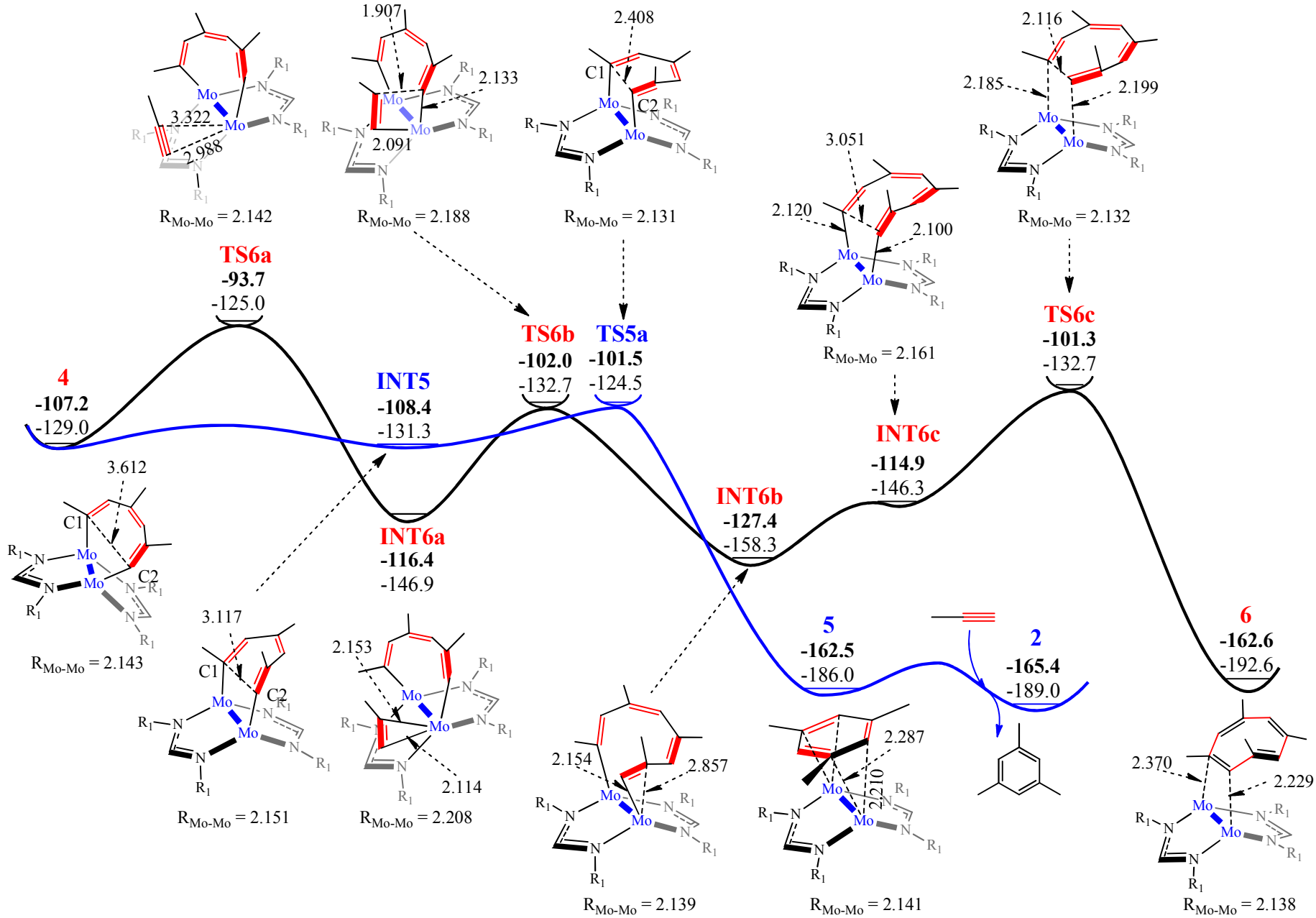

Figure 7. The energy change in the reductive elimination of benzene and [8+2] cycloaddition between **4** and propyne.

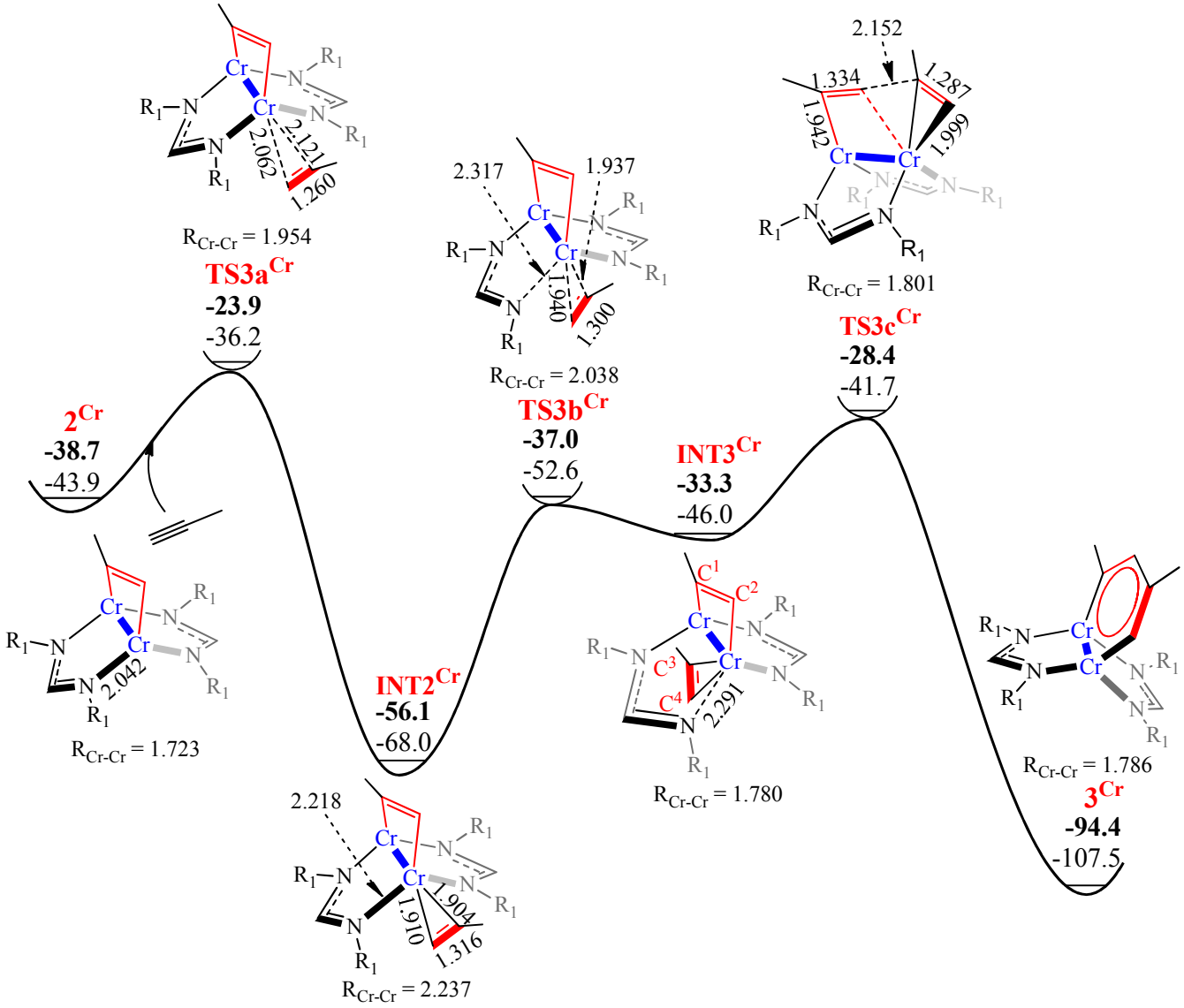

Figure 8. The energy change in the [4+2] cycloaddition between **2**^{Cr} and propyne.

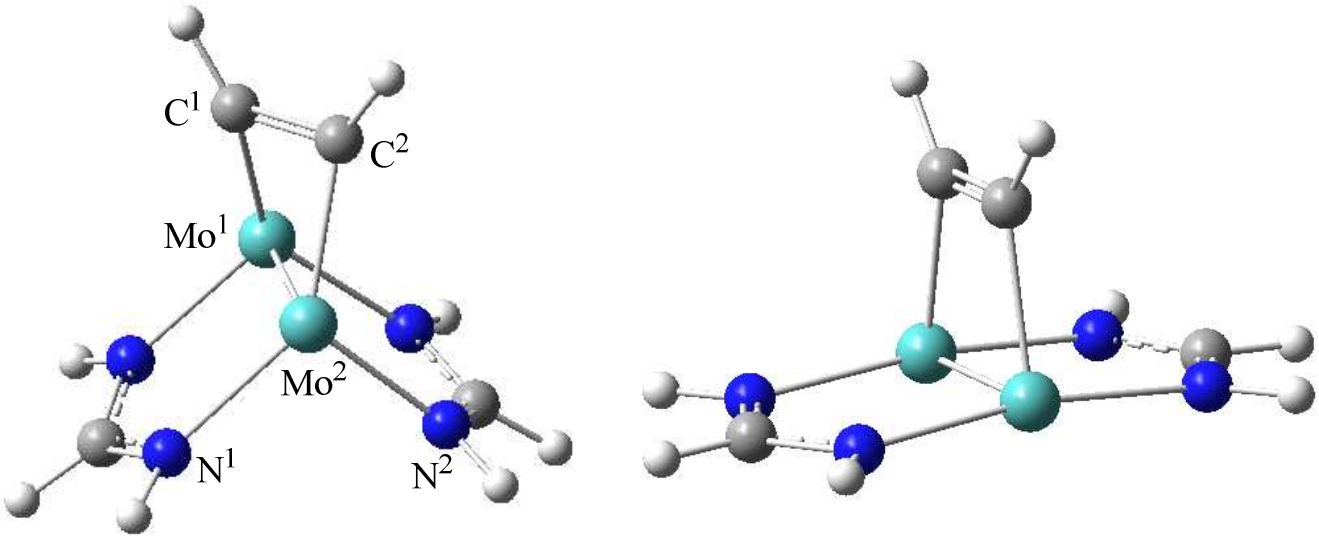

$\varphi(C^1\text{-}Mo^1\text{-}Mo^2\text{-}C^2) = -27.1$
$\angle(N^1\text{-}Mo^2\text{-}N^2) = 98.0$
-42.6 kcal/mol
2a^m

$\varphi(C^1\text{-}Mo^1\text{-}Mo^2\text{-}C^2) = 0.0$
$\angle(N^1\text{-}Mo^2\text{-}N^2) = 175.7$
-25.7 kcal/mol
2b^m

Figure 9. Planar and non-planar structures of four-member ring complex **2^m**.

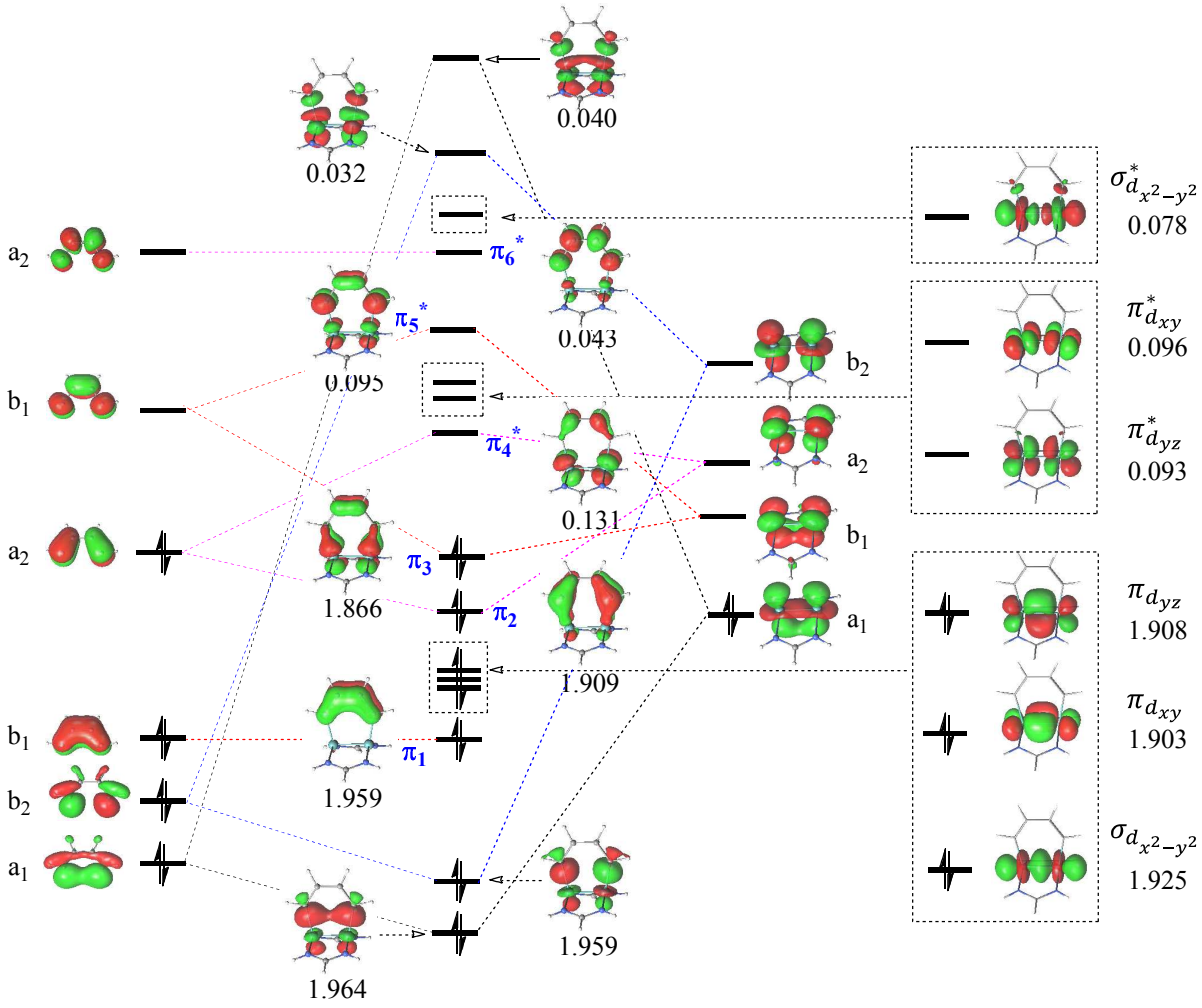

Figure 10. Natural orbitals and occupation numbers of **3** calculated by the RASSCF(16e,16o) method**.**

Graphical Abstract: The reaction mechanism of catalytic synthesis of benzene from alkynes by Mo-Mo quintuple bond and electronic structure and bonding nature of dimetallacyclobutadine and dimetallbenzyne were study theoretically.